LEGIBILITY NOTICE

A major purpose of the Technical Information Center is to provide the broadest dissemination possible of information contained in DOE's Research and Development Reports to business, industry, the academic community, and federal, state and local governments.

Although portions of this report are not reproducible, it is being made available in microfiche to facilitate the availability of those parts of the document which are legible.

3

Los Alamos National Laboratory is operated by the University of California for the United States Department of Energy under contract W-7405 ENG-36

LA-UR--89-2162

DE89 014285

TITLE COMPETING INTERACTIONS AND COMPLEXITY IN CONDENSED MATTER

AUTHOR(S) A. R. Bishop, T-11

SUBMITTED TO Proceedings of NATO ISI "Partially Integrable Systems" Les Houches, France, March 1989 (Academic Press)

DISCLAIMER

Los Alamos Los Alamos National Laboratory
Los Alamos, New Mexico 87545

COMPETING INTERACTIONS AND COMPLEXITY IN CONDENSED MATTER

A. R. BISHOP
Theoretical Division and Center for Nonlinear Studies
Los Alamos National Laboratory
Los Alamos, NM 87545, USA

ABSTRACT. Some major themes of space-time complexity in condensed matter contexts are reviewed. They are illustrated through model and physical systems, analysed by both analytical and numerical techniques.

1. Introduction

Two of the main directions that can be clearly discerned in current dynamical systems research are: (1) A return to the reality of ***spatially extended*** dynamical systems studied by a variety of novel techniques, including neural networks, cellular automata and coupled map lattices, as well as direct numerical integration of partial differential equations (pde's) and coupled ordinary differential equations (ode's); and (2) Recognition of the central role played by ***competing interactions*** (both of length and time scales) in pattern formation and complex dynamics.

Here we will introduce examples of, and approaches to, these issues in *condensed matter* contexts. Complexity in both time and space are important in condensed matter for device performance, response and transport properties, etc. However, condensed matter also provides excellent vehicles to probe general issues in dynamical systems. This is because of the availablity of controlled materials, small scale experiments, and sophisticated probes of both time and space [1,2].

Broadly three classes of problems might be distinguished -- these are separated mostly by historical developments and happily they are growing together as we focus increasingly on the real materials provided by nature. Nevertheless, it is easier to appreciate previous literature by separating:

(a) ***Structural Complexity*** in *classical* equilibrium Hamiltonian systems with competing (incommensurate) interactions or periods -- the analog of temporal problems with two or more incommensurate frequencies. The competing length scales lead to a variety of nontrivial, spatially inhomogeneous ground states and transitions, and there are by now many physical observations in widely varying experiments [3]. The inhomogeneous ground states often have the form of superlattice structures (e.g. of soliton arrays) similar to texturing in some metallurgical contexts [4]. Perhaps the biggest open question here is to understand *dynamics*, particularly large scale flow in such problems -- this is usually "glassy" and "hysteretic." Indeed much of materials science concerns the roles of "defects" in controlling both strength and flow.

(b) ***Nonlinear pde's and coupled ode's***, again mostly classical, including effects of *external* forcing which naturally introduces competitions for length and time scales. Issues here include [1] the coexistence of coherence and chaos, the use of nonlinear spectral methods [5] to identify collective excitations, the importance of generalized homoclinic orbits [6], and the qualitatively new effects that can be induced by noise and disorder. Again, there are now many natural as well as more

contrived experimental studies which are closely mimicked by such pde's and their equivalents (cellular automata, etc.) [1].

(c) *Quantum Hamiltonians* can also arise naturally in solid state and statistical physics. These offer some new approaches to probing the poorly understood area of "quantum chaos," i.e., quantum behavior of integrable and nonintegrable models with interesting (e.g. chaotic) classical limits. Recent examples here include quantum spins [7] and exciton-phonon coupled systems [8]. The focus is on gaining control of nonintegrability and $\hbar$ as "tuning" parameters, and studying wave-function structure and evolution as well as energy level distributions.

We should also emphasize the probable interconnectedness of the classes above. Indeed in a number of cases formal *mappings* can be identified between time-dependent and equivalent Hamiltonian systems (in a higher spatial dimension) or quantum models. In this way the central role played by competing interactions is revealed. Thus, for example, the inhomogeneous "ground states" referred to in (a) contain the character of "intermittency" observed in appropriate regimes of (b). The reader is referred to [9] for more details.

By way of illustrating some of the above phenomena, techniques and outstanding issues, we mainly focus here on the *sine-Gordon* (SG) and closely related cubic nonlinear Schrödinger (NLS) equations in the presence of various kinds of perturbations. SG has been a template of nonlinear pde's for many years because: (1) In its pristine (1 + 1)-dimensional form it is strictly integrable. This means that elegant analytic techniques (e.g. nonlinear spectral analysis [5]) for isolating true "solitions" are available, which has given insight into ideas of "collective coordinates" and "particle-like" solutions of wider applicability. Further, we are able to identify the deviation from integrability as a controlled parameter; and, equally importantly, (2) SG represents a *class* of nonlinear Klein-Gordon equations which arise naturally in many branches of physics [10]. Nature is often quite closely modeled (on many spatial scales) by coupled nonlinear oscillators, and solitons or solitary waves can control transport, statistical mechanics, localization, radiation absorption frequencies, etc.

As a simple example consider the problem of "current oscillations" in the dynamics of near-commensurate systems [11]. The 1 + 1 dimensional driven, damped SG equation,

$$\ddot{\varphi}(x,t) + \alpha\,\dot{\varphi}(x,t) - \ddot{\varphi}'(x,t) + \sin\varphi(x,t) = \Gamma\ , \tag{1}$$

has been used as a model for, e.g. charge-density-waves or a vortex lattice in a superconductivity film whose thickness is periodically modulated in one-direction. In eq. (1) the overdot is $\partial/\partial t$, the prime is $\partial/\partial x$, α is a damping parameter, and Γ is a DC-driving field. The boundary conditions may be, e.g., periodic or periodic mod (2π) to allow for a fixed average density of kinks (dicommensurations), n_k. If $n_k = 0$ the problem is said to be commensurate while $n_k \neq 0$ measures the deviation from commensurability. The observable "current" $\langle \dot{\varphi} \rangle = L^{-1} \int dx\ \dot{\varphi}(x,t)$. Physically, the commensurability is between two characteristic length scales. Thus in the charge density wave case $\varphi(x,t)$ corresponds to the phase field of the order parameter (a periodic lattice and charge density distortion induced by electron-lattice coupling) and the charge density wave with a commensurability wavelength Ma/N (with M, N reduced integers and a the lattice constants) has the form $\sim \cos(2\pi Nx/Ma + \varphi)$. This charge density can couple to the component of the lattice potential with periodicity a/N and produce an interaction energy $\sim \cos(M\varphi)$, thus $\varphi \to M\varphi$ in eq. (1). In the incommensurate case the charge density wave has the form $\sim \cos(2\pi N/Ma + \delta q)x + \varphi$ with the interaction energy $\sim \cos(M\varphi + Mx\delta q)$

x); thus $\varphi(x) = M_0 + M_1 \delta q\, x$ and δq determines the boundary condition in eq. (1). In the case of the vortex lattice $\varphi(x,t)$ is a center of mass field, the pinning force $\sim \sin \varphi$ is due to the thickness modulation, and eq. (1) corresponds to deviation of the vortex average spacing (determined by an applied magnetic field) from the period of the thickness modulation. Further details and references concerning both of the above problems can be found in [11].

There are now *numerous* numerical and analytical studies of the SG equation in different dimensions and under a variety of physically relevant perturbations. We record here only a few *representative* source references [1,5,12].

The remainder of this report describes a selected sequence of problems in more detail. Section 2 is devoted to the (1+1)-dimensional SG with spatially uniform AC-driving and damping. Section 3 considers the same problem but with DC-driving instead. Section 4 introduces a discrete SG system but with nonconvex interparticle interactions, admitting an internal competition of length scales. Section 5 returns to a *single* particle problem but, by including quantum effects, raises questions of whether the scaling and statistical approaches to "chaos" developed for classical problems can be useful in the quantum domain. Section 6 contains a brief summary and some concluding remarks.

Although, we are concerned here with problems motivated by condensed matter, the dynamical systems issues are of course much more general. This report should be read in conjunction with those of e.g., Coullet, Ghidhalgia, Newell, Ribotta and Pomeau.

2. Sine-Gordon Equation with Damping and ac-Driving: A Quasi-Periodic Route to Chaos in a Near-Integrable PDE

Solutions of nonlinear evolution equations often exhibit rich patterns in space and time which may have both coherent and chaotic components. In both dissipation-dominated and near-conservative cases, the solutions reside in an infinite dimensional phase space but may approach attractors which are low-dimensional. Hence, the mathematical techniques developed in recent dynamical systems theory are hopefully relevant. In particular, these techniques explain how motion near a low dimensional attractor of a deterministic system can act chaotically, and they offer means to characterize the nature of the attractor quantitatively. On the other hand, techniques from modern nonlinear partial differential equations provide coordinates for the attractors. These coordinates capture coherent spatial patterns of the solutions. It is certainly natural to try to combine insight from these two approaches.

We focus in this section on near integrable nonlinear wave equations. The underlying integrability provides a wide selection of solutions for potential nonlinear resonances, and it offers sufficient structure for the possibility of analytical coordinates for the attractors. Thus, near integrability provides the analytical tools for a precise description of near conservative phenomena, some of which appear more generic in near conservative cases than the integrable methods might suggest.

For near integrable problems a strategy is to find a nonlinear resonance, and then to study the system in a neighborhood of this resonance. Here we study, as an example, the damped, ac driven sine Gordon equation under periodic boundary conditions [5]:

$$\varphi_{tt} + \alpha\varphi_t - \varphi_{xx} + \sin\varphi = \Gamma\cos(\omega t), \qquad (2.1)$$

$$\phi(x + L, t) = \phi(x, t), \tag{2.1b}$$

$$\phi(x, t = 0) = \phi_{in}(x), \tag{2.1c}$$

$$\phi_t(x, t = 0) = v_{in}(x). \tag{2.1d}$$

Here $0 < \varepsilon \ll 1$, and the control parameters, are α (the strength of the dissipation), Γ (the amplitude of the ac driver), ω (the frequency of the ac driver), L (the spatial period), and the initial data (ϕ_{in}, v_{in}).

For the purposes of illustrations we further specialize here to the case where the frequency ω is near, but less than, unity,

$$0 \ll \omega \lesssim 1. \tag{2.2}$$

This choice places us in a "nonlinear (cubic) Schrödinger (NLS) regime"; that is, when $\omega \lesssim 1$, one can use singular perturbation methods to approximate a class of equations, which includes the sine-Gordon equation (1.1), by a NLS equation. Elsewhere [13], we have studied lower driving frequencies (e.g. $\omega \simeq 0.6$) for which the NLS approximation is not valid; in these regions of parameter space, the chaotic attractors are dominated by "breather" to "kink-antikink" transitions (see 2B below). Here, in the NLS regime, we will see that the attractors are dominated by similar, but distinct, collective-mode transitions, namely breather-radiation interactions.

Classical dynamical systems diagnostics applied to the results of careful numerical experiments have identified (in a particular parameter range) intermittency between quasi-periodic and chaotic states. We have used soliton modes to begin an effective coordinatization of the attractors, capturing both their temporal and spatial structures. This is done through a nonlinear spectral transform which permits several new conclusions. It: (1) confirms that even the chaotic attractors can be well described by a few soliton modes; (2) establishes the existence of homoclinic orbits in the underlying integrable problem; (3) measures the presence of homoclinic crossings in the perturbed system; and (4) shows the importance of soliton interactions in the transitions between metastable parts of the attractor. Thus, far more precise information is now available about the nature of the onset of chaos for this near integrable example than can ever be expected for pde's with less structure.

First we summarize the results of extensive numerical experiments [5]. The global picture of transitions in the NLS regime is depicted in the schematic diagram of fig. 1. Before describing the space-time structures in each region of this diagram, we first set the stage for these experiments. The parameters in the system (2.1) were chosen as: $\varepsilon = 0.1$, $\alpha = 0.4$, and $L = 24$. The remaining parameters are then varied: ω is varied below, but near, unity, and Γ is varied near 0. The initial conditions $\phi_{in}(x)$, $v_{in}(x)$ are taken to be a whole-line sine-Gordon breather localized inside the period L, and extended periodically to the whole line.

In the "quasi-periodic" regime III of fig. 1 there are also windows of subharmonic locking rather than true quasi-periodicity — a familiar situation in two frequency dynamical systems (e.g. circle maps). In fact around $\omega \sim 0.9$ the quasi periodicity is suppressed completely (see fig. 1) and an unusual transition from regime II to IV occurs directly.

Pertinent questions about the bifurcation sequencies in fig. 1 include: what is the origin of the second frequency in the quasi-periodic region?; how does this second independent frequency correlate with the increased spatial structure?; do

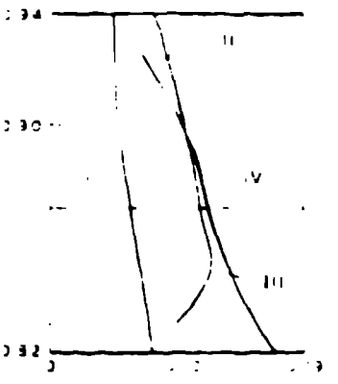

Figure 1. Semi-schematic bifurcation diagram for the ac-driven damped SG equation in the NLS regime. Other parameter values are $\varepsilon\alpha = 0.04$ and $L = 24$. The final attractors are shown as functions of driving frequency (ω) and strength ($\varepsilon\Gamma$) and labeled as: I, period, locked to the driver (x-independent); II, period, locked to the driver (one localized breather); III, quasiperiodic (weak period L/2 state superimposed on II); and IV, chaotic, with intermittent laminar regions (competition between two breathers and anharmonic L/2 radiation).

these spatial structures have a meaningful, quantitative interpretation in terms of the exact sine-Gordon theory?; does the dynamics in these regions (including region IV) admit to a perturbation analysis of the integrable sine-Gordon equation?

To be specific we focus on parameter values $L = 24$, $\varepsilon = 0.1$, $\varepsilon\alpha = 0.04$ and $\omega = 0.87$, with initial data a SG breather with frequency parameter $\omega_{br} = 0.77$. The control parameter for the experiment is Γ, the amplitude of the ac driver $-$ ($\varepsilon\Gamma$) ranges over (0.0, 0.116). For purposes of orientation, this experiment is represented by a line in fig. 1.

The attractor in this bifurcation experiment may be represented as Γ increases by the symbolic sequence

$$\begin{pmatrix} FLAT, \\ PERIODIC \end{pmatrix} \rightarrow \begin{pmatrix} PERIOD\ 1, \\ PERIODIC \end{pmatrix}$$

$$\rightarrow \begin{pmatrix} \sim PERIODIC\frac{1}{2} \\ QUASI-PERIODIC \end{pmatrix} \rightarrow \begin{pmatrix} \sim PERIODIC\frac{1}{2} \\ CHAOTIC \end{pmatrix},$$

which we abbreviate by

$$(F, P) \rightarrow (P1, P) \rightarrow (\sim P\frac{1}{2}, QP) \rightarrow (\sim P\frac{1}{2}, C).$$

For small driving amplitudes ($0 < \varepsilon\Gamma < 0.0585$) the periodic spatial structure of the initial breather decays as a transient, and the attractor is an x-independent flat state with no spatial structure, which is periodic in time. This state is locked to the AC driver with its temporal period. The existence and stability of this locked state can be established with classical mathematical analysis, both with and without the NLS approximation. For example in the NLS approximation, the field ϕ is represented as

$$\phi(x,t) = \sqrt{6\varepsilon}\{A(T, \sqrt{\varepsilon}x)e^{it} + c.c.\}, \tag{2.3}$$

where the complex amplitude $A(T, X)$ satisfies the driven, damped NLS equation

$$-2iA_T + A_{XX} + 3|A|^2A = i\alpha A + \Gamma', \quad \alpha(1-\omega)\Gamma, \tag{2.4}$$

where $\Gamma' = \Gamma/2\sqrt{6\varepsilon}$. A flat locked state is represented by a solution of this equation in the form

$$A(X,T) = Ce^{-i(1-\tilde{\omega})T/2} \quad , \tag{2.5}$$

where the complex constant C satisfies

$$[-(1-\tilde{\omega}) + 3CC^*]C = i\alpha C + \Gamma^{\varepsilon} \quad . \tag{2.6}$$

A typical hysteresis diagram depicting the solutions of this algebraic equation, together with the stability of the locked state (2.5) to arbitrary perturbations with spatial period L, is shown in ref. [5]. Note in particular that the flat state on the lower branch is stable to all perturbations, while the state on the upper branch can become unstable, at large enough Γ values, to spatially dependent perturbations. These instabilities are long wavelength modes; the short wavelength modes are always stable. As the amplitude of the flat locked state increases, the most unstable mode changes from a flat ($\kappa = 0$) state, to a $\kappa_1 = 1(2\pi/L)$ state, on to a $\kappa_2 = 2(2\pi/L)$ state, etc.

As we increase Γ, the amplitude of the flat attractor rises along the lower branch, until it reaches a "knee" in the hysteresis curve at $\varepsilon\Gamma \simeq 0.1015$. For large values of Γ, the attractor must change. In fact, for $\varepsilon\Gamma \in (0.0585, 0.1015)$, one stable attractor is a single excitation within each period, superimposed on a flat background. The existence and stability of this (P1,P) state can be established by mathematical analysis. Γ is further increased, all of the attractors develop instabilities at shorter wavelength. The first such instability is a $\kappa = 2$ mode, with spatial wavenumber $\kappa_2 = 2(2\pi/L)$. Thus, we anticipate that the locked breather state will become unstable, as Γ is increased, to $P\frac{1}{2}$ states.

As Γ is further increased beyond $\varepsilon\Gamma = 0.1015$ the attractor becomes quasi-periodic in time and appears to be characterized spatially by the same single breather, but now accompanied by a $\kappa = 2$ radiation-like excitation. As $\varepsilon\Gamma$ approaches 0.1053 from below, the upper threshold of the ($\sim P\frac{1}{2}$, QP) attractor, the amplitude in the $\kappa = 2$ radiation visibly increases and initial transient times increase. The long transients, because of their large $\kappa = 2$ component, often appear as approximate $P\frac{1}{2}$ spatial structures in the sense that two coherent excitations are present in the spatial period. Indeed, at large dissipation, a locked two-breather state, periodic in time, is achieved, instead of a quasi-periodic state -- energy is permanently transferred from $\kappa = 1$ to $\kappa = 2$.

For $\varepsilon\Gamma \geq 0.1053$, the $P\frac{1}{2}$ tendency in the above transient persists for all time and is visibly enhanced: at times the attractor appears as two localized breathers per spatial period, and and at other times as extended $\kappa = 2$ anharmonic radiation. The overall temporal behavior is now chaotic, with intermittent visitation of a small number of distinct metastable parts of the attractor. Broadly speaking the attractors consist of at least two metastable parts: (1) striking "laminar" regimes, which are essentially the same as the quasi-periodic attractors ($\sim P\frac{1}{2}$, QP) of the prechaotic regime, which occur at smaller $\varepsilon\Gamma$ values; and (2) intermittent chaotic bursts. However, upon closer inspection, these chaotic bursts reveal substructure characterized by a dynamical energy exchange between (a) predominantly $\kappa = 2$ radiation, and (b) two-breather states per period. In addition some of the dynamics and transitions between metastable parts of the attractor are accompanied by *relative* motion of the coherent components of the $\sim P\frac{1}{2}$ structure. As the threshold $\varepsilon\Gamma = 0.1053$ is approached from above, the fraction of time spent in laminar regions increases.

These features of the bifurcation sequence are substantiated by the use of many standard diagnostics from dynamical systems theory. Namely: (i) time series of spatially averaged quantities ($H = \frac{1}{2}\,\varphi_t^2 + \frac{1}{2}\,\varphi_x^2 + 1 - \cos\varphi$, and displacement φ); (ii) phase planes for $\mathbf{P}(t) = (\varphi(x_1,t), \varphi(x_2,t))$, with x_1 and x_2 arbitrarily chosen points on the chain; (iii) Poincaré sections (using variables as in (ii) to define a plane in a three-dimensional phase space); (iv) temporal power spectra, $S(\cdot\cdot\cdot\omega)$, at $x_1 = 0$ (the center of the chain); (v) leading Lyapunov exponent (computed from two initially neighboring trajectories with a distance norm $n = \int_0^L (\varphi_t^2 + \varphi_x^2)dx$); (vi) the correlation dimension computed according to the algorithm of Grassberger and Procaccia. Complete details may be found in [5]. As an example we show simple time series in fig. 2. Note in particular: (1) in the quasi-periodic cases, the modulation of the time signal by the second (lower) frequency and the growth of the amplitude of this modulation with increasing Γ; (2) in the chaotic case (fig. 2a), temporal intermittency characterized by the presence of laminar regions separated by (chaotic) bursts; (3) the quasi-periodic nature of these laminar regions (cf. figs. 2b) and the linear growth with time of the *modulational* amplitude; (4) the very similar <H> values (or modulational amplitudes) at which all laminar regions are exited.

These and other [5] conventional dynamical systems diagnostics yield temporal information. For a partial differential equation such temporal data should be correlated with spatial information. One possibility is a linear spectral analysis in κ-, as well as ω-, space. For near integrable nonlinear pde's such as that discussed here, more insight is gained from a *nonlinear spectral analysis*, correlated with space-time profiles.

First, we briefly describe the nonlinear transform. For more complete detail, see refs. [14]. The method may be summarized as follows: at time t; we take the (numerically) generated spatial profile $\{\varphi(x,t)|\forall x \in [0,L]\}$ and numericallly perform a spectral transform to obtain $\{\hat{\varphi}(\lambda,t)|\forall\lambda\}$. This transform maps the field from its spatial representation *onto a representation on a basis of solitons*, in terms of which the unperturbed sine-Gordon equation is exactly separable. Thus the spectral representation $\hat{\varphi}(\lambda,t)$ measures precisely the number, types and physical characteristics of the solitons (the localized coherent states) which are present in the wave at time t. If the temporal dynamics were the perfect sine-Gordon equation, these spectral properties would be invariant in time. However, because of the perturbations, they change with t and must be measured successively at t increases.

This transformation from the "spatial representation" $\{\phi(x)\}$ to the spectral representation $\{\hat{\varphi}(\lambda)\}$ is defined through a linear, non-self-adjoint eigenvalue problem, with spectral parameter λ lying in the complex plane. For periodic φ, the spectrum of this eigenvalue problem is entirely continuous spectrum residing on curves in the complex λ-plane. The real axis is always spectrum, and complex spines of spectrum attached to the real axis are associated with excited "radiation-like" modes in $\varphi(x)$. In particular a spine near $\lambda^2 = \frac{1}{16}$ indicates the presence of a long wavelength mode; while spines near $\lambda^2 \simeq 0$ and $\lambda^2 \simeq \infty$ correspond to modes with high spatial wave number k. Curves of spectrum in the complex λ plane which are not tied to the real axis are associated with soliton wavetrains in φ. These coherent excitations come in two types, namely kink (and/or antikink) trains and breather trains. Kink trains are associated with bands of spectrum on the imaginary λ axis; breather trains are associated with a pair of bands in the

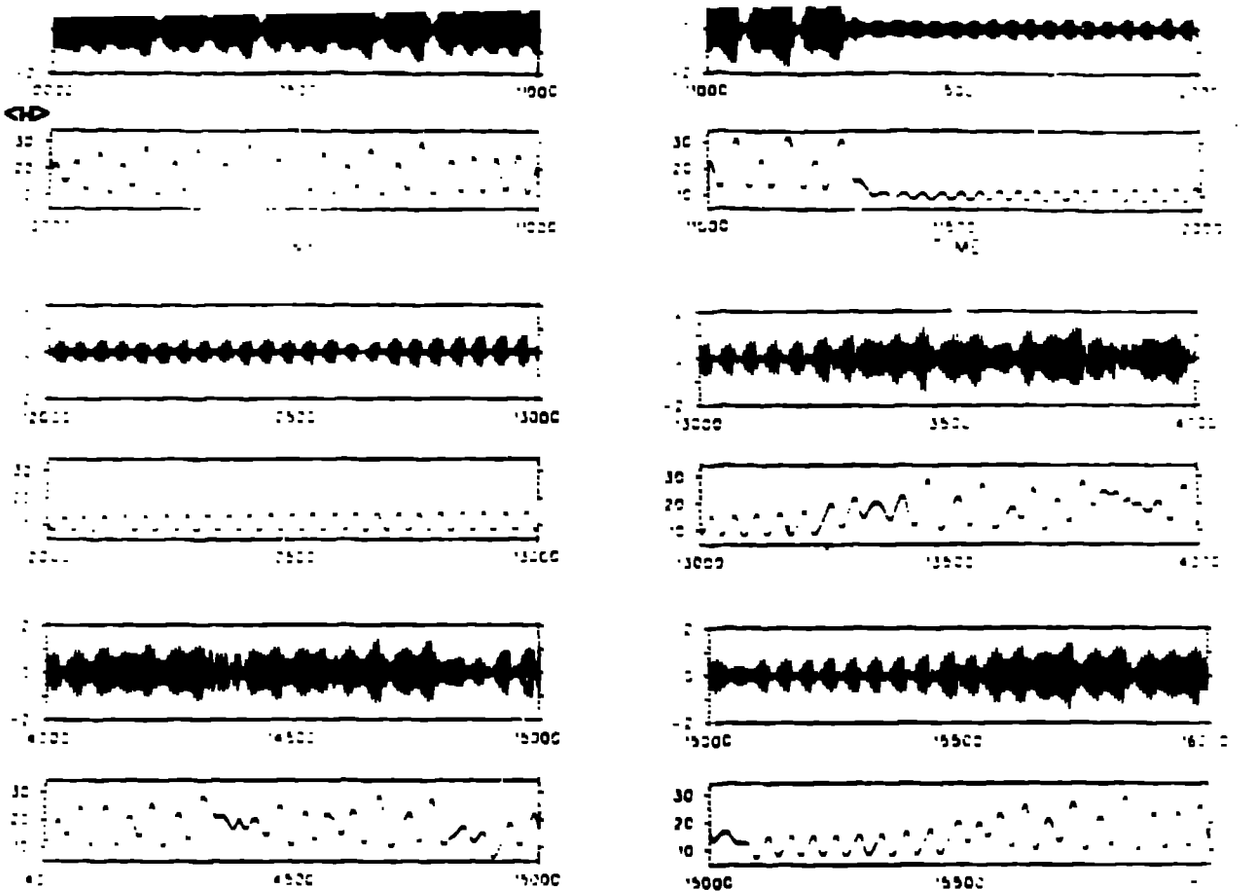

Figure 2. Time series for spatially-averaged SG energy ⟨H⟩: $H = \frac{1}{2}\sum_i \sigma_i^2 - \frac{1}{2}\sum_{\langle ij \rangle} \sigma_i \sigma_j - \sum_i h_i \sigma_i$ and field ⟨σ_i⟩: *above*: $\epsilon\Gamma = 0.1055$ (intermittent chaos); *below*: (top left): $\epsilon\Gamma = 0.101$ (periodic); Lower left: 0.102 (weakly quasi-periodic); 0.1055 (top right: small, and lower right: large, amplitude "quasi-periodic" laminar intervals from chaotic case (above)).

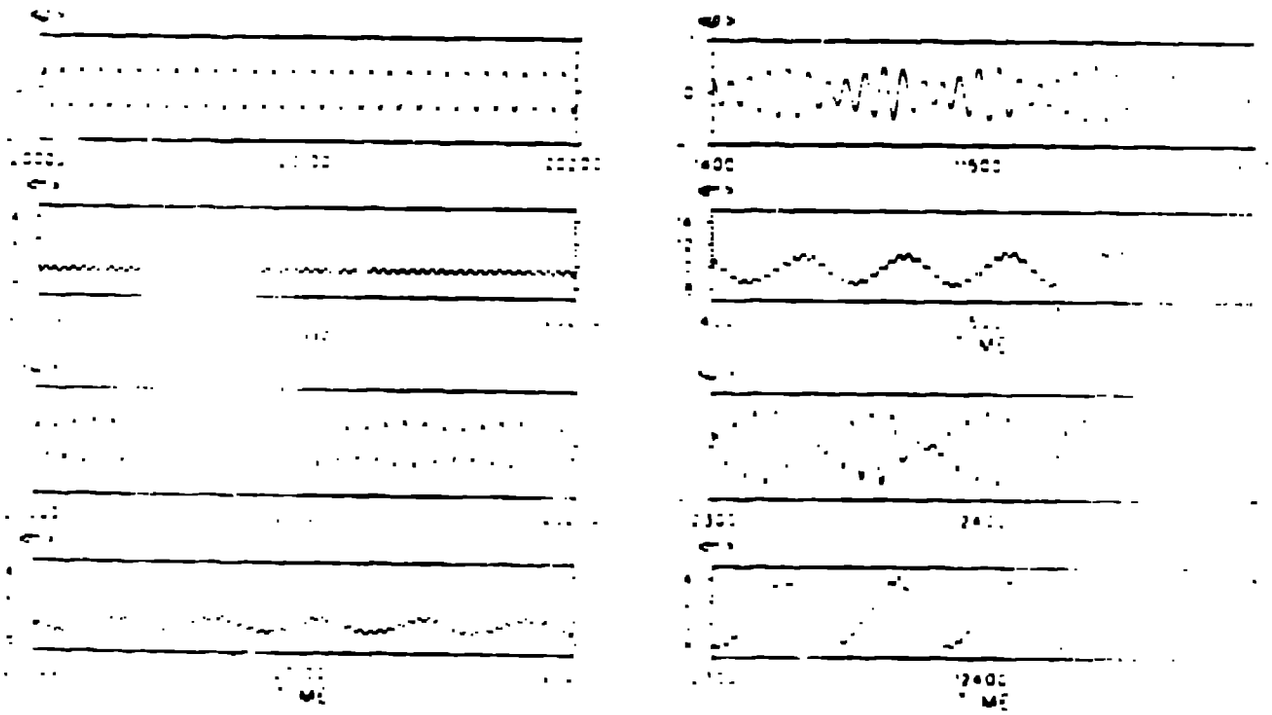

first and second quadrants, and their complex conjugates. In the NLS regime, where displacements of ϕ are small (compared with 2π), only breather trains are accessible.

Given $\phi(x)$, the spectrum of the linear eigenvalue problem is actually determined through the "Floquet discriminant" $\Delta(\lambda, \phi)$, an analytic function of both ϕ and the spectral parameter λ. The spectrum comprises those curves in the complex λ plane for which $\Delta(\lambda)$ is real and $-2 \leq \Delta(\lambda) \leq 2$. It is these curves of spectrum which are depicted in the figures shown below. Several additional remarks are necessary in order to interpret these figures:

i) Typically, bands of spectrum off the real axis are very short. If one band were to degenerate to a point in the upper half λ plane (which cannot happen for periodic potentials), a soliton would be present in ϕ. An isolated point on the imaginary axis $\lambda = i\nu$ would indicate a kink (or antikink) which would evolve under sine-Gordon dynamics with velocity $(1 - 16\nu^2)/(1 + 16\nu^2)$. An isolated point in the first quadrant would indicate a breather with sine-Gordon velocity $(1 - 16|\lambda|^2)/(1 + 16|\lambda|^2)$ and an internal breather frequency $\nu = \cos[\tan^{-1}(\lambda_I/\lambda_R)]$. Because the bands of spectrum are so short, these facts about solitions are useful qualitative approximations even in the periodic case.

ii) Excitations with spectrum inside the circle of radius $\frac{1}{4}$ travel to the right, while those with spectrum outside this circle travel to the left.

iii) Symmetries of ϕ imply symmetries in its spectrum. Since ϕ is real, its spectrum comes in quartets: if λ belongs to the spectrum, so do $-\lambda$ and $\pm\lambda^*$. Thus, it is sufficient to examine the closed first quadrant in the complex λ plane. In addition, if ϕ and ϕ_t are chosen to be even functions of x (here about $x = 0$) this additional symmetry induces another symmetry in the spectrum about the circle of radius $\frac{1}{4}$: namely, if λ belongs to the spectrum so does $1/(16\lambda)$.

iv) In these figures, "." denotes a band of spectrum where $-2 \leq \Delta(\lambda) \leq 2$. Points λ_p, where $\Delta(\lambda_p) = +2$, are denoted "⊞"; points λ_0, where $\Delta(\lambda_0) = 0$, are denoted "0"; points λ_a, where $\Delta(\lambda_a) = -2$, are denoted "◇". Note also that the associated spatial profiles $\phi(x)$ and $\phi_t(x)$ are induced as inserts in the spectral plots, with the solid lines representing ϕ and the dotted lines ϕ_t.

We now return to the bifurcation sequence at $\omega = .87$. First consider $\Gamma = 0.101$ which is in the (P1,P) regime of one excitation in each spatial period, locked temporally to the $2T$ driver. Fig. 3 shows the nonlinear spectrum of the locked state at three instants in time. It detects one breather at rest in the laboratory frame, riding over a flat ($\kappa = 0$) background. The curve of spectrum associated to this breather is located on the circle of radius $\frac{1}{4}$, at an angle of $\sim 30°$ with the real axis. No radiation modes, other than $\kappa = 0$, are visible, although numerical data shows that low κ modes are very weakly excited, increasingly so as $\varepsilon\Gamma$ approaches the quasi periodic threshold ($\varepsilon\Gamma \simeq 0.1015$). This spectrum is not t-independent, as it is for completely integrable SG dynamics, but it executes $O(\varepsilon)$ fluctuations. For instance the breather spectrum oscillates periodically with the driving frequency between $\sim 29°$ and $\sim 32°$. This small periodic fluctuation in the spectrum is consistent with the small temporal oscillation of $\langle H \rangle$, fig. 2.

As $\varepsilon\Gamma$ is increased into the quasi-periodic regime to a value of 0.104, the $P\frac{1}{2}$ character accompanying the single breather is clearly visible in the spatial profiles (see fig. 4a). In the nonlinear transform of these profiles, the $\kappa = 2$ mode is now visibly excited, as well as weaker modes of shorter wavelength. In addition, a particularly interesting new feature is present in the nonlinear spectra for this case. Namely, at times the spine of spectrum associated to the breather merges with that

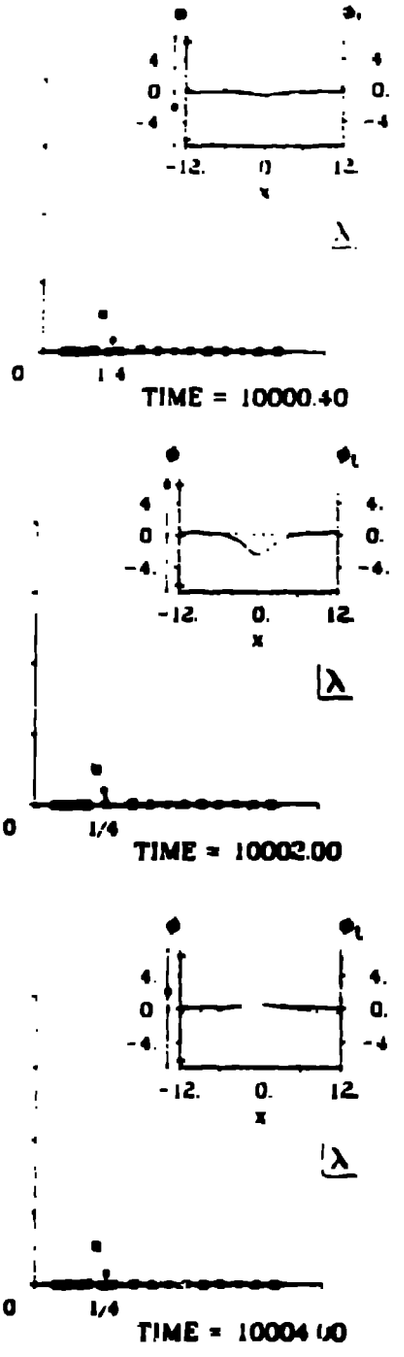

Figure 1. ... spectral transform of the ...P1.P0 attractor at ...Γ = 0.1... ... only one half of the ... period.

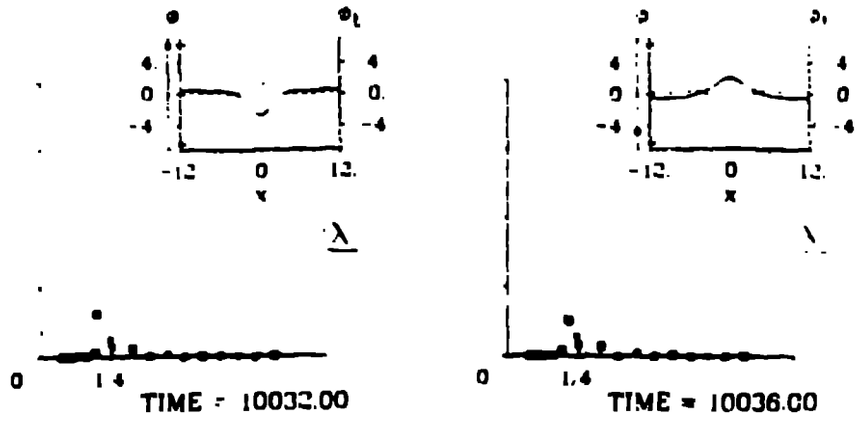

a

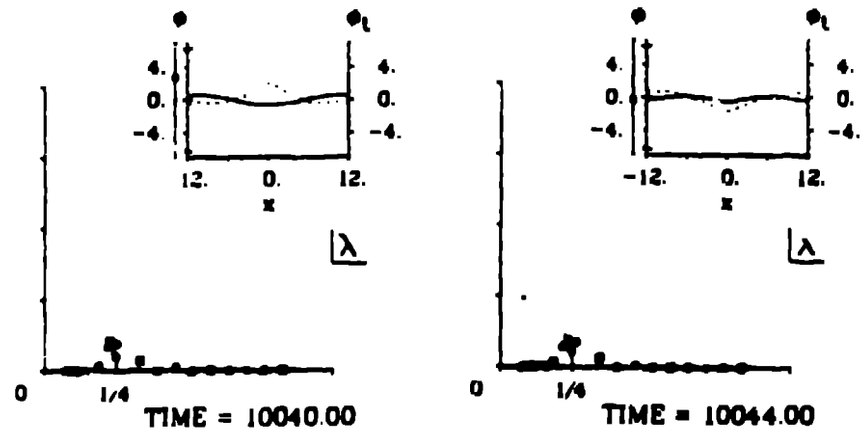

b

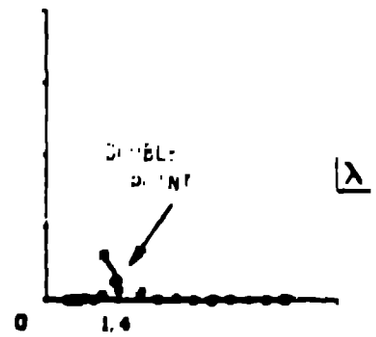

c

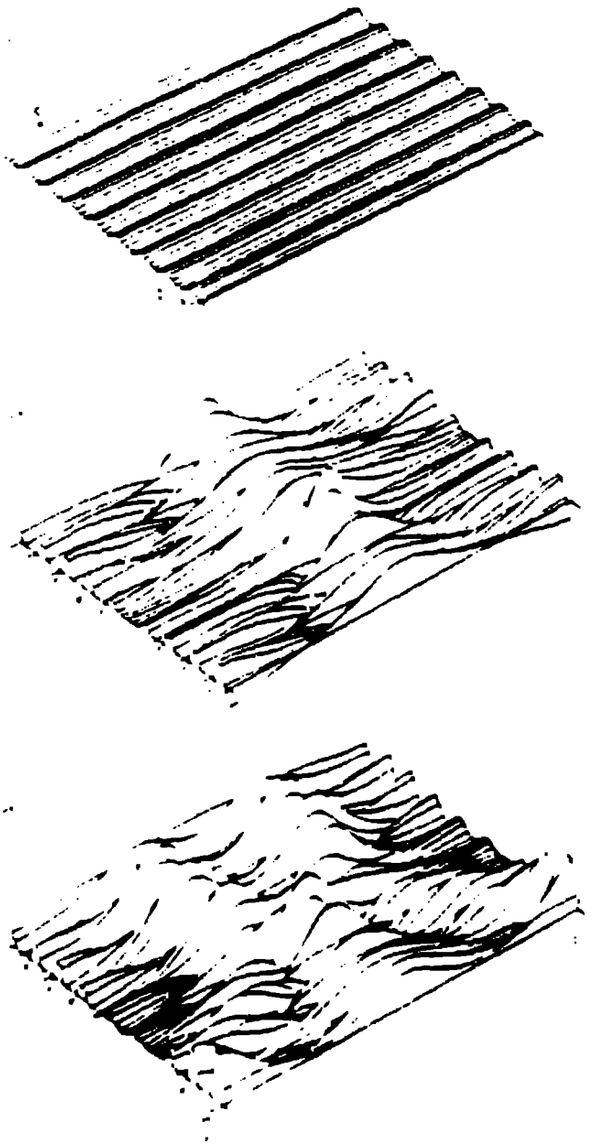

Figure 7. Space-time profiles at $\omega = 0.87$ and $\Gamma = 0.050$ (flat in space-periodic case), $\Gamma = 0.105$ (quasi-periodic case), $\Gamma = 0.110$ (chaotic case). Note the secondary wavelength $\lambda = L/2$ in the quasi-periodic case and the changes in spatial symmetry in the chaotic case.

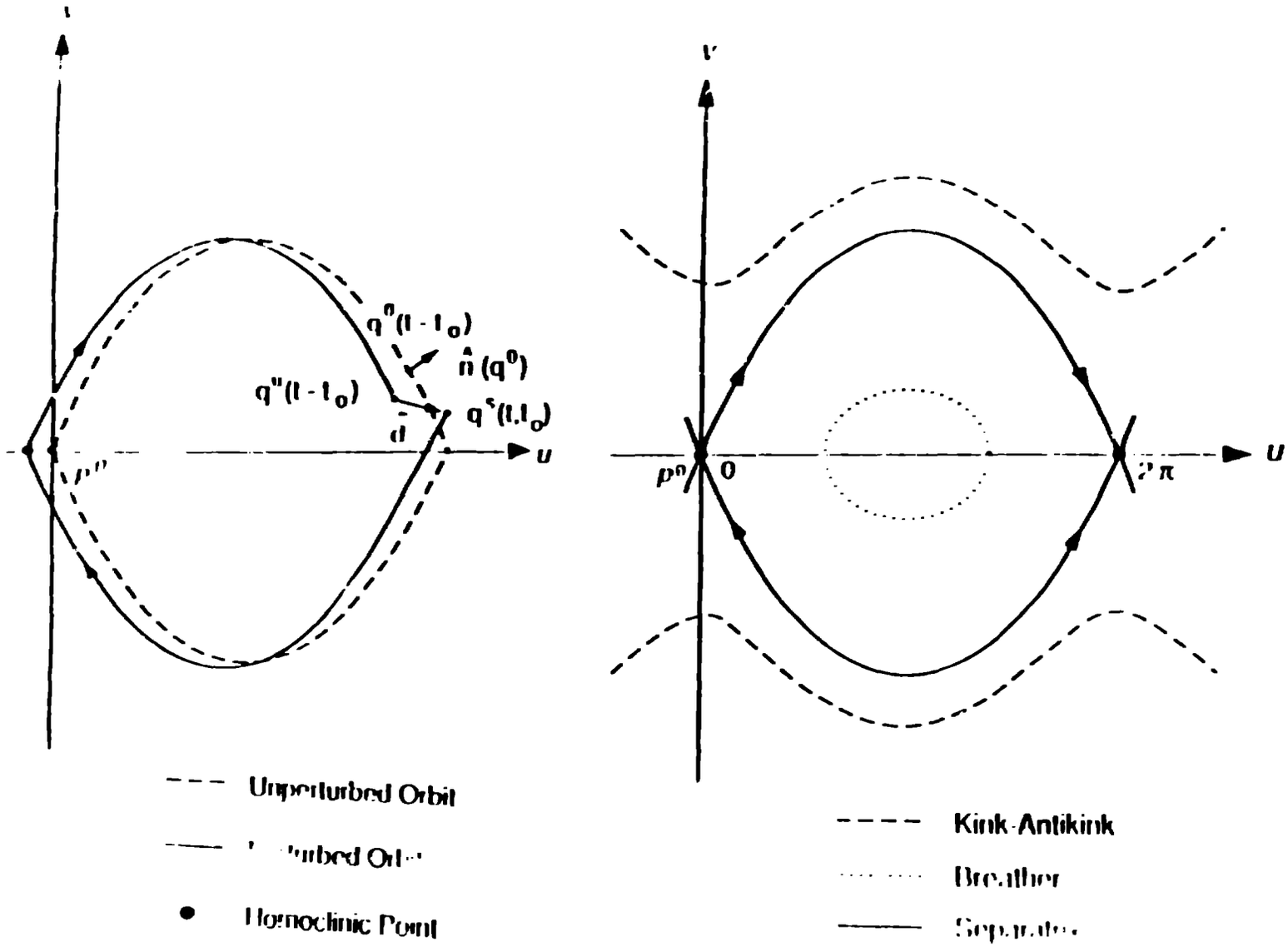

Poincaré Surface of Section Poincaré map for the system under consideration. The closed orbits correspond to [illegible] while the unbounded orbits correspond to kink antikink pair motion. The separatrix [illegible] the amplitude just attains 2π as a kink antikink pair with zero relative velocity [illegible] In this figure, the points 0 and 2π are identified as the [illegible] Melnikov distance [illegible] the perturbed orbit

spine attached to the real axis at $\lambda = \frac{1}{4}$ (and associated with the background) and at later times (fig. 4b) becomes a "cross" of spectrum. This cross corresponds to the presence of "periodic" extended $\kappa = 1$ anharmonic radiation mode in the profile. Oscillation in the spectrum between the "cross" and "breather" curves occurs regularly in t, with the period of the *slow* underlying modulation. Thus, these spectral measurements show that the state oscillates (on a slow scale) between that of a predominantly coherent breather (fig. 4a) and that of a predominantly extended $\kappa = 1$ anharmonic radiation (fig. 4b), each accompanied by $\kappa = 2$ radiation. The transitions between these coherent breather and extended radiation states are correlated with the oscillations in <H>, which are now of larger amplitude (see fig. 2): the maxima of <H> correspond to the breather configurations, while the minima of <H> correspond to extended states.

The breather configuration and the extended configuration are separated by a state which is a ***homoclinic orbit*** under pure sine-Gordon dynamics. It is analogous to the separatrix in the single pendulum's phase space in that it has infinite temporal period. As discussed in refs. [6,15,21] homoclinic crossings play a central role in the chaotic regime just as for the single pendulum. Here the homoclinic states separate in phase space states with distinct spatial structures -- in the present case breather from radiation, and in other cases (see below) kink-antikink from breather.

Detailed nonlinear spectral analysis of the chaotic regime in fig. 1 can be found in Ref. [5]. A major conclusion is that, just as for the quasi-periodic precursor regime above, even the chaotic attractor (at least near the chaotic threshold) can also be described by a few ($\sim$ 3-4) nonlinear modes. The basic scenario quantified by nonlinear spectral analysis is captured in the space-time profiles shown in fig. 5. In the chaotic (intermittency) regime, energy is nonlinearly transferred from the k=1 breather to the nonlinear k=2 mode which grows into two independent and oppositely moving breathers. These breathers bounce and interact irregularly (through the periodic boundary conditions) and eventually annihilate each other. This results in k=1 nonlinear radiation which resynchronizes into a breather plus k=2 radiation and (irregularly) repeats the cycle. This collective nonlinear mode formation and dynamics is isolated very clearly by the nonlinear spectral analysis applied at various stages of the intermittency.

It is important to note that the nonlinear transform demonstrates that *both* coherent and extended (radiation) modes are necessary to coordinatize the quasi-periodic and chaotic attractors. Further, in the chaotic regimes, the motion and interaction of coherent structures, accompanied by self-consistent radiation modes, describe both the metastable states and transitions between them.

An ultimate test of the approach outlined above will of course be the use of "soliton collective coordinates" in analytic descriptions of transitions to and qualities of "chaos." This program is now making substantial progress in several respects, including: (i) extension of proofs of finite dimensional inertial manifolds (previously developed for linear mode bases [16]) to soliton bases [17]; and (ii) use of soliton coordinates to describe homoclinic orbits, connections in the presence of perturbations, and e.g., Melnikov tests for homoclinic tangles in some extended systems [18,19] -- again generalizing results available for single particles [20]. These works are not yet mature enough to review here. However, some of the ideas can usefully be introduced through two model problems: (A) A linear mode truncation of damped SG with *high* frequency driving, and (B) A collective coordinate reduction for single breather KK breakup in the damped SG with *low* frequency driving.

2(A). Correlations Between Chaos in a Perturbed SG Equation and a Truncated Model System

Here we summarize a recent study [21] of the same high frequency driving, damped SG system as above but with a shorter line (L = 12). This length is found to support only *one* breather excitation and thus finds an even simpler route to chaos. Specifically, with symmetric initial data and periodic boundary conditions, a discrete (bimodel) symmetry has been imposed −− a breather may synchronize equally well at its seed position or a distance L/2 away. Chaotic dynamics appears as a flattering between these locations via a "flat" state. The same nonlinear spectral analysis as above supports this picture and again identifies intermediate states that are O(1) unstable and correspond to homoclinic states in the integrable (i.e. unperturbed) limit. It is then natural to surmise that the chaotic dynamics on these attractors is due to the perturbation of these homoclinic configurations. The purpose of this section is to introduce a model dynamical system that mimics such behavior and which has proven analytically tractable. The model is derived by a low-order *linear* mode truncation of the nonlinear Schrödinger equation. Such a truncation is generally very dangerous. However its regimes of validity can be monitored here by the parallel use of the nonlinear spectral transform on the full pde.

Considering eqs.(2.1) again we use $\varepsilon\alpha = 0.04$ and $\omega = 0.87$ but, as mentioned above, L = 12. As expected the system resonates with a *low* amplitude breather-like spatial mode accompanying a k = 0 flat motion. In this low amplitude regime we can easily derive a perturbed nonlinear Schrödinger envelope as a good approximation: ($\omega \equiv 1 - \varepsilon\tilde{\omega}$). Writing

$$\phi = 2(\varepsilon\omega)^{1/2}[B(X,T)e^{i\omega t} + c.c.] + O(\varepsilon) \tag{2.7}$$

$$X = (2\varepsilon\omega)^{1/2}x \quad ; T = \varepsilon\tilde{\omega}t \ ,$$

the slowly varying envelope B(X,T) satisfies

$$iB_T + B_{XX} + (|B|^2 - 1)B = i\alpha B + \Gamma \ . \tag{2.8}$$

Note that this amplitude equation has preserved an integrable unperturbed limit (the cubic NLS) and has factored out one frequency (that of the driver, ω). Thus steady solutions of (2.8) correspond to frequency locked solutions of (2.1), while periodic flows of (2.8) which are incommensurate with ω, correspond to quasi periodic perturbed SG solutions.

Based on the numerical observation of a low amplitude breather on a flat background, we examine a further severe mode truncation of (2.8):

$$B(X,T) = a(T) + b(T)\cos(kX) \ , \tag{2.9}$$

$$k = 2\pi/L \ , \qquad L = L(2\omega)^{1/2} \ .$$

Inserting (2.9) into (2.8) and retaining cubic terms in the complex Fourier amplitudes a(T), b(T) yields

$$a_T + \ldots a^2 + \frac{1}{2}b^2 \ldots + \ldots \frac{1}{2}b^2 \ldots a^*ba \quad \text{conj.} = \Gamma \tag{2.10}$$

$$-ib_t + (|c|^2 + \frac{3}{4}|b|^2 - (1+k^2))b + (cb^* + bc^*)c = i\tilde{\alpha}b \ .$$

This 4-dimensional dynamical system is of course not expected to be in *quantitative* agreement with the full p.d.e. and the effect of including an additional mode is discussed in Ref. [21]. However: (i) it has guided intuition on the nonlinear soliton mode basis in the presence of the same perturbations, both in terms of geometric phase space structure and connections, including implementation of Melnikov tests [18,22]; and (ii) the ansatz (2.9) has proven capable of modeling several of the features observed in the full p.d.e., including the chaotic fluttering of a weakly unstable breather, via an intermediate flat O(1) unstable state, mentioned above. Specifically, the 2-mode ansatz admits the symmetry (c,b) → (c,-b), corresponding to a translation of ϕ by L/2, and b = 0 is an invariant subspace which corresponds to the flat intermediate structure. In the nonlinear spectral language, the ansatz is robust enough to capture all three key spectral configurations of the "gap" state, the "cross" state, and the intermediate state with complex double points and associated homoclinic character.

Very importantly, the *unperturbed* limit of the truncated system is an integrable Hamiltonian system, with two real independent integrals:

$$I \equiv |c|^2 + \frac{1}{2}|b|^2 \tag{2.11}$$

$$H \equiv \frac{1}{2}|c|^2 + |b|^2|c|^2 + \frac{3}{16}|b|^4 - \frac{1}{2}(1+k^2)|b|^2 - |c|^2 + \frac{1}{4}(b^2c^{*2} + b^{*2}c^2) \ .$$

Complete analytical analysis of fixed point structure and stability are possible as well as explicit solution by quadrature [21]. Furthermore, a direct correspondence can be established between the o.d.e. fixed points and SG solutions. For instance, the ring of fixed points $(c,b) = (e^{i\phi}, 0)$ $(\phi \in [0, 2\pi])$ in the b = 0 invariant subspace corresponds to $\phi \sim 2(\varepsilon\omega)^{1/2}[c\, e^{i\omega t} + c^*\, e^{-i\omega t}]$, describing the flat (pendulum) solution frequency-locked to the driver. The fixed points are readily found to be O(1) unstable, reflecting the same O(1) instability of the flat SG solution. Moreover, the orbits homoclinic to the ring reflect the SG solutions which are homoclinic to the pendulum solution with frequency $\omega = 0.87$. In fact identifying the integral

$$h \equiv H - (\frac{1}{2}I^2 - I) \tag{2.12}$$

we can readily find an effective oscillator equation for $Z \equiv B^2$ $(b = B\, e^{i\theta})$,

$$\frac{1}{2}Z_T^2 + \frac{Z^2}{32}(Z - 8k^2 + 7Z - 8(2 - k^2)) + h = 0 \tag{2.13}$$

with infinite period solution: $0 < Z < 8(2 - k^2)$, $k^2 < 2$.

Other fixed points of the o.d.e. system can similarly be assigned in the full p.d.e. A complete bifurcation and stability picture for the *perturbed* o.d.e. system has been determined numerically and many of the key elements can be derived analytically or by straightforward perturbation theory [21].

The correspondence of homoclinic crossings in the o.d.e. and p.d.e. has been checked in several ways. In the perturbed p.d.e. these crossings are measured by

following the exact nonlinear SG spectrum of ϕ at each time step and identifying transitions from "gap" to "cross" states (c.f. fig. 4). In the o.d.e. system we have followed $h = H - \frac{1}{2}I^2 - I$) and checked for zero crossings. As a final check we have combined these two diagnostics. We take c(T), b(T) during the flow generating h, reconstruct the perturbed SG solution according to the approximation (2.7), and then compute the SG spectral components of ϕ. The question is whether h passing through zero corresponds to the SG field ϕ passing through a homoclinic spectral configuration? As shown in [21] the agreement is indeed rather good except very near to the homoclinic structure ($h \simeq 0$), as might be expected due to the approximation by linear Fourier modes.

Recent analysis of the truncated model suggests [22] that a homoclinic loop (rather than a tangle) is responsible for chaos in this system. Interestingly it appears that the geometric structure of the model problem can indeed by lifted to soliton variables and applied to the full perturbed SG and NLS p.d.e.'s

Finally, we note that the model problem introduced here is in fact a particular case (with somewhat different perturbations) of a general class of problems introduced by Holm et al. [23], motivated by polarization dynamics in nonlinear optical beams. Detailed discussions of reductions to finite-dimensional inertial manifolds, homoclinic crossings, chaos and Arnol'd diffusion have also been given by these authors.

2(B). A Mode Reduction for the Breather -- Kink-Antikink Transition and Associated Chaotic Dynamics

We now turn to an equally drastic approximation for chaos via a second homoclinic crossing in the SG equation, namely the breakup of a breather into a counterpropagating kink-antikink pair. This scenario has also been explored in great detail numerically [12,13] although usually not associated with an underlying homoclinic structure. It is especially relevant with lower frequency AC-driving since this induces resonant breathers with large amplitude $\lesssim 2\pi$. Although the collective coordinate scheme we introduce [24] is much oversimplified, it turns out to be surprisingly successful. It will also serve to introduce the basic ideas of homoclinic orbits and Melnikov's criterion for the onset of complexity. In general p.d.e.'s pose problems of coexisting homoclinic structures and connections, and far more general phase space geometry than in an o.d.e. However the basic ingredients in chaos really are one-dimensional in the present problem and captured by breather/kink-antikink collective coordinates.

Specifically, we consider here a one-dimensional SG system in which a single breather excitation is present. When this system is perturbed by spatially uniform DC and AC driving, and space-independent dissipation, the breather can break into a kink-antikink (KK) pair, which can then recombine into a breather soliton. This process may occur repeatedly, with a frequency that is not necessarily related to that of the driver. To understand this competition, consider the breather and KK solutions to the unperturbed SG equation:

Breather:

$$\phi_B(x,t) = 4\tan^{-1}\left\{\frac{\tan\theta\,\sin[\nu(t)]}{\cosh[2k(x - x_0(t))]}\right\}, \qquad (2.14)$$

$$\nu(t) = \nu_0 + t\ cos\theta\ ,$$

$$k = \frac{1}{2}\ sin\theta\ ,$$

$$E_B = 16\ sin\theta\ ,$$

$K\bar{K}$:

$$\phi_{K\bar{K}}(x,t) = 4\ tan^{-1}\left\{\frac{sinh[u(t-t_0)\sqrt{1-u^2}}{u\quad sh[(x-x_0)/\sqrt{1-u^2}]}\right\}\ , \tag{2.15}$$

$$E_{K\bar{K}} = \frac{16}{\sqrt{1-u^2}} > 16, \quad u \geq 0\ .$$

Here, ν_0, x_0 and $0 \geq \theta < 2\pi$ are constants, u is the $t \rightarrow \infty$ velocity of the kink and -u is the $t \rightarrow \infty$ velocity of the antikink. From Eqs. (2.14) and (2.15), we see that the breather's internal frequency, ω_B, is $\cos\theta$. The breather soliton can be viewed as the bound state of a kink-antikink pair, with threshold binding energy $\Delta E = 16(1 - \sin\theta)$, and where $u \rightarrow 1/(2\tan\theta)$ and $t_0 \rightarrow -\nu_0/\cos\theta$. Now, if the system supports a breather excitation, and is externally driven by $\gamma\ \sin\omega t$, and damped by $\alpha\partial\phi_B/\partial t$, then the rate of change of the system's energy is $\dot{H} \approx \gamma\ \sin\omega t \int dx(\partial\phi_B/\partial t) - \alpha \int dx(\partial\phi_B/\partial t)^2$, so that $\dot{H}$ can be either positive or negative. When $\dot{H}$ is positive, enough energy can be fed into the system that the breather attains $E = 16$, and breaks into a $K\bar{K}$ pair. Likewise, if $\dot{H}$ is negative, the $K\bar{K}$ pair may lose enough energy to recombine into a breather.

The specific equation under consideration is eq. (2.1) which we write as

$$\phi_{tt}(x,t;\varepsilon) - \phi_{xx}(x,t;\varepsilon) + sin\ [\phi(x,t;\varepsilon)] = \varepsilon F(t,\phi_t)\ ; \tag{2.16}$$

where $\varepsilon F(t,\phi_t)$ is the perturbation,

$$\varepsilon F(t,\phi_t) = \eta(t) - \alpha\phi_t(x,t;\varepsilon)\ ; \tag{2.17}$$

$$\eta(t) = \Gamma + \gamma sin\omega$$

$$\varepsilon = max\{\alpha, \Gamma, \gamma\}\ .$$

Here, the variables x and t denotes space and time, respectively, while subscripts x and t denote partial derivatives w.r.t. these variables. Also, ε is the overall strength of the perturbation, Γ represents the DC driving, $\gamma\ \sin\omega t$ denotes the AC driving and $\alpha\Phi_t(x,t;\varepsilon)$ is the damping.

In order to investigate this pattern competition in Eq. (2.16), we make a severe mode truncation to the breather collective coordinates, which leads to a three dimensional set of o.d.e.'s which may then be analyzed by Melnikov's method [20]. Salerno has shown [25] that this procedure yields a system whose separatrix dynamics is equivalent to the separatrix dynamics of the full p.d.e. Several interesting predictions have been obtained [24] for space time instabilities in this system. In particular, the perturbation can result in transverse crossings of the stable and unstable orbits to the homoclinic point, which corresponds to intermittent bursts

and unbinding of the KK pair. This is indeed the basic nature of low-dimensional chaos, and has been observed numerically [13] for the AC-driven, underdamped sine-Gordon eq. in when the frequency of the driver is low.

Complete details of this analysis can be found in ref. [24]. Here we only sketch the basic steps.

First we must determine equations of motion for the collective coordinates. This can be achieved within several perturbative approaches. One such approach is to take the ansatz that the solution to the perturbed SG equation has the same form as the unperturbed breather, Eq. (2.14), except that now we allow θ and x_0 to be functions of time, so that

$$x(t) = x_0(t) + \int^t dt' cos\theta(t') \ . \tag{2.18}$$

By making this approximation, we are assuming that the perturbation is sufficiently weak that its main effect on the system is to continuously alter the phase and the frequency of the breather. Since the breather energy is intimately related to its frequency ($E_B = 16\sqrt{1-\omega_B^2}$), we see that this is valid when $\omega_B \ll 1$. Next, we introduce the breather collective coordinates, (u(t;ε), v(t;ε)), where

$$\begin{aligned} u(t;\varepsilon) &= \phi_B(x = x_0, t; \varepsilon) \\ &= 4tan^{-1}A(t) \end{aligned} \tag{2.19}$$

and

$$\begin{aligned} v(t;\varepsilon) &= \left.\frac{\partial \phi_B}{\partial t}\right|_{x=x_0} \\ &= \frac{4\dot{A}(t)}{1+A(t)^2} \ , \end{aligned} \tag{2.20}$$

where $A(t) = \tan\frac{\theta}{4}\sin x_0(t)$.

In terms of $A(t)$ and its time derivatives we have

$$\begin{aligned} \dot{u} &= v \\ \dot{v} &= 4(\ddot{A}\cos^2(u/4) - 2(v/4)^2 \tan(u/4)) \ . \end{aligned} \tag{2.21}$$

To obtain the equations of motion for the breather collective modes, $\ddot{A}$ must be found in terms of $u(t;\varepsilon)$, $v(t;\varepsilon)$. After substantial algebra this may be obtained to consistent perturbative order, and, introducing

$$Z \equiv \tan\frac{u}{4}, \qquad W \equiv \dot{Z} \ ,$$

we can be written as the following autonomous dynamical system:

$$\dot{Z} = W$$

$$\dot{W} = \varepsilon f(Z) + \varepsilon^2 g(Z) \ ,$$

(2.22)

with

$$\vec{\chi} = \begin{pmatrix} z \\ w \end{pmatrix} :$$

$$\vec{f}(\chi) = \begin{pmatrix} w \\ -\frac{z(1-w^2}{1+z^2} \end{pmatrix}$$

$$\varepsilon\vec{g}(\vec{\chi};t) = \begin{pmatrix} 0 \\ \tilde{\eta}(t)g_\eta(z,w) - \alpha q_\alpha(z,w) \end{pmatrix} .$$

where

$$\begin{aligned} g_\eta(z,w) &= \frac{1}{(1+sw^2)(w^2+z^2)(1+s)\sqrt{1+z^2}} \\ &\times \left[\left(w^2+z^2\right)z^2 - s\left\{z^4 + w^2\left[z^2 + \left(1-w^2\right)\left(1+z^2\right)\right]\right.\right. \\ &\left.\left. + 2w^2z^2s^2\left(1+z^2\right)^2 + w^2s^2\left(1-2z^2\right)\left(1+z^2\right)^2\right] \end{aligned}$$

and

$$\begin{aligned} g_\alpha(z,w) &= \frac{w}{(1+sw^2)(w^2+z^2)(1+z^2)} \\ &\times \left[\left(2+z^2\right)\left(w^2+z^2\right)z^2\right. \\ &- s\left\{z^4 - w^2\left[\left(2+z^2\right)z^4 - \left(1-w^2\right)\left(1+z^2\right)\right]\right\} \\ &\left. + w^2s^2\left(1+2z^2\right)\left(1+z^2\right)\right] . \end{aligned}$$

In order to study the onset of irregular behavior in this system, we consider the Poincaré map, P^t, where $t_0 \in [0, 2\pi/\omega)$, fig. 6. The distance, $d(t_0)$, between the perturbed stable and unstable orbits to the homoclinic point is given by Eq. (4.5.11) in Ref. [20]:

$$d(t_0) = \frac{1}{\left|f\left(q^0(t_0)\right)\right|} M(t_0) , \qquad (2.23)$$

where

$$f\left(q^0(t_0)\right) = w^2 = \frac{z^2(1-w)^2+1/2}{(1+z^2)^2} ,$$

and $M(t_0)$ is the Melnikov function

$$M(t_0) = \int_{-\infty}^{\infty} dt\, f\left(q^0(t-t_0)\right) \wedge g\left(q^0(t-t_0);t\right)$$

$$\exp\left[\int_0^t dt' Tr\, D_x g\left(q^0(t'),t'\right)\right]$$

In the definition of $d(t_0)$, q^0 is the unperturbed separatrix orbit, $\vec{f} \wedge \varepsilon\vec{g}$ is the exterior product of $\vec{f}$ and $\varepsilon\vec{g}$ ($\vec{f} \wedge \varepsilon\vec{g} = \sum \varepsilon_{ij}\, f_i \varepsilon g_j = f_1 g_2 - f_2 g_1$, with ε_{ij} the Levi-Civita tensor), and $Tr\{Df(q^0(t'))\}$ is the trace of the Jacobian matrix of $\vec{f}$ evaluated on the separatrix.

$$Tr\{Df(\vec{\gamma})\} = 0 + \frac{2w z}{1+z^2} .$$

The separatrix orbit is easily determined from Eq. (2.22). From the second component,

$$\dot{w} = z = -\frac{z(1-w^2)}{1+z^2} ,$$

we see that z changes sign when $w = \dot{z} = \pm 1$, so that, on the separatrix,

$$z = \pm(t - t_0)$$

and

$$w = \pm 1 . \tag{2.24}$$

The upper (resp. lower) sign corresponds to the upper (lower) orbit in fig. 6.

When Eqs. (2.22) and (2.24) are substituted into Eqs. (2.23), we get

$$d(t_0) = \int_{-\infty}^{\infty} \frac{dt}{(1+s^2)} \left(1+t^2\right)^{-7/2}$$

$$\left\{ \vec{\eta}(t+t_0)\left[\left(1+s\right)\left(1+t^2\right)t^2 + \right.\right.$$

$$2t^2\left(1+t^2\right)s^2 + \left(1+t^2\right)^2\left(1-2t^2\right)s^3\Big]$$

$$-\alpha\frac{1+s}{\sqrt{1+t^2}}\left[t^2\left(2+t^2\right)\left(1+t^2\right)\right.$$

$$\left.\left. - st^4\left(1-t^2\right) + s^2\left(1+t^2\right)\left(1+2t^2\right)\right]\right\} , \tag{2.25}$$

where $\gamma(t+t_0) = \frac{\pi}{T}\{\Gamma + \gamma\sin[\omega(t+t_0)]\}$. Expanding $\sin[\omega(t+t_0)]$ and using the fact that $\ldots$ even in t, Eq. (2.25) has the form

$$d(t_0) = M(t_0) = \frac{\pi}{T}[\Gamma m_0 + \ldots p\omega \ldots \sin\omega t_0] - \alpha m_1 , \tag{2.26}$$

where m_0 and m_1 are numerical constants, and p is a function of ω only [24]. The zeros of the Melnikov function then yield the parameter values for which the stable and unstable manifolds to the homoclinic point intersect, so that "complicated" heather kink antikink behavior may occur whenever

$$\frac{\gamma}{\alpha} > \left(\frac{\gamma}{\alpha}\right)_{crit} = \frac{1}{p(\omega)}\left(\frac{\Gamma m_0}{\gamma} - \frac{\Gamma m_1}{\alpha}\right) \tag{2.27}$$

Since our primitive soliton mode truncation has excluded the possibility of exciting radiation modes, the breather in the full p.d.e. may destabilize at a lower driving strength. In fact, the competition between a single breather state and a two-breather state, mediated by a radiative state has been observed for periodic SG. Notice that the threshold for breather breakup is a monotonic increasing function of the driving frequency. This can be seen by realizing that we are looking at motion near the separatrix, so that $\omega \approx 0$ is close to the frequency of the breather, and energy is efficiently fed into the system. When the driving frequency is nearly one, we are far off resonance, and the amplitude of the driving must be large.

From Eq. (2.27) we see that the effect of adding DC driving to the system is always to decrease the threshold for breather breakup (m_Γ is positive). This is readily understood: The addition of spatially homogeneous, time-independent driving to the SG equation may be viewed as the addition of a term of the form $-\Gamma\phi$ to the potential, 1 - cosϕ. When $V(\phi) = 1-\cos\phi-\Gamma\phi$ is plotted versus ϕ, we see that small amplitude motions correspond to breather states, while large ϕ solutions correspond to kink solitons. Since the DC contribution decreases the potential, thereby making large-amplitude solutions possible at lower energies, addition of DC driving will enhance the soliton conversion.

Surprisingly the numerical values of $(\gamma/\alpha)_c$ calculated by this method agree with previous numerical work quite well. For example, with $\alpha = 0.2$, $\omega = 0.6$ the threshold for intermittent chaos is $\gamma \simeq 0.9$ [13], i.e. $\gamma/\alpha \simeq 4.5$. The Melnikov criterion developed here predicts $(\gamma/\alpha)_c = 4.4$.

3. Sine-Gordon Equation with Damping and dc-Driving: A Model Transverse Instabilities on Propagating Interfaces

We now turn to spatially uniform DC driving instead of the AC-driving of the previous section. This may appear much less interesting. However, especially with *weak* damping the pattern formation, hysteresis and complex dynamics is in fact extremely rich.

The phenomena basically described by this equation include zero-field steps in Josephson junctions, spontaneous nucleation of kink-antikink pairs in stressed materials, and transverse structures on propagating domain-wall interfaces. The last example includes such systems as charge-density-wave materials, magnetic-flux-flow systems, and many other phenomena appearing in the presence of a nonlinear, periodic potential. While we stress the wide applicability of our results, we shall present this section in the language of Josephson junctions for concreteness.

The structure of zero-field steps (ZFS's) in overlap-geometry Josephson junctions has been the subject of many theoretical and experimental studies. With recent advances in materials technology, it has become possible to manufacture these junctions in other configurations — notably, in an annular geometry. From a theoretical point of view, this geometry has important advantages, since an analysis of periodic SG can make use of rigorous analytical results, such as inverse-scattering theory. This situation gives us the opportunity to study issues that are central to dynamical systems theory for spatially extended systems (such as space time complexity, pattern formation, pattern competition, and mode conversion) from both a well established theoretical framework, and in a controlled physical system.

The results that we present here [26] are for the one dimensional, DC driven SG equation with dissipation, viz

$$= \varepsilon o_t(x,t) - \Gamma_0 \ , \qquad (3.1)$$

with periodic boundary conditions,

$$o(x,t) = o(x+L,t)$$

and

$$o_\xi(x,t) = o_\xi(x+L,t) \ .$$

Here, $o_\xi = \partial o/\mathrm{d}\xi$, and $\xi = x$ or t. In Eqs. (3.1), x is the spatial variable, normalized to the Josephson penetration depth, λ_J [$\lambda_J = \hbar/2\mu_0 \epsilon J d$, where $\hbar$ is Planck's constant, μ_0 is the magnetic permeability of the vacuum, ϵ is the electron charge, J is the maximum pair-current density and d is the magnetic thickness of the insulating layer]. Also, t is the time variable, in units of the inverse plasma frequency, $1/\omega_J$ [$1/\omega_J = (\hbar C/2J\epsilon)^{1/2}$, where C is the capacitance per unit area of the junction]. On the right-hand side of Eq. (3.1), Γ_0 is the DC-driving, and εo_t represents the dissipation (this is the only form of damping considered here). In Eq. (3.1), L is the length of the system. For our numerical studies, we take $\varepsilon = 0.1$, $0 \leq \Gamma_0 \leq 1.0$, $L = 24$, and consider a fairly discrete system, with 76 lattice sites.

As we shall see below, this system possesses a rich variety of multisoliton wavetrains and transitions between them, including the same breather-KK breakup discussed in section (2B). First we summarize the results of a numerical study [26]. Fig. 7 presents data in the form of current ($=\Gamma_0$) versus voltage ($=\ll o_t \gg$, in our normalized units, where the double angular brackets denote averages over space and time). This picture was generated by starting with a stationary, large-amplitude, spatially-random profile, with $\Gamma_0 = 1.0$. We then permitted the system to evolve in time according to Eqs. (3.1) until it reached a $t \to \infty$ attractor; the homogeneous-spatial profile. The driving, Γ_0, was then "adiabatically" reduced to zero, to generate the backbone of the curve. Each of the steps was then developed by starting with the state at which an abrupt drop in voltage occurred, and then increasing the driving "adiabatically" until the voltage abruptly jumped to the power-balance regime — in this portion of the I-V curve, the energy input by the dc driving matches the time-averaged dissipation. (The arrows on the curves in this figure indicate the direction in which Γ_0 was changed to trace out the steps.)

From Fig. 7, we see that the system displays a number of interesting features. The most prominent of these is the existence of two different transport mechanisms. In the high-voltage steps immediately below the power balance, or McCumber curve, the transport occurs through cavity modes (which are standing waves of phase-locked, multibreather wave trains), where current flows because a standing wave is superimposed on a running average (see Fig. 8). In the language of solitons, this running average is due to the fact that during its oscillation, $o(x,t)$ crosses a potential energy at each instant that its spatial profile is flat. On these steps, the amplitude and wavelength increase as the step number decreases. In the region of low voltage, the standing waves have developed a full 2π amplitude, and have increased the number of active modes by delocking the phases of the breathers. Then sustained K K pairs are nucleated, thereby giving transport by the *transverse motion* of kinks. Notice that the imposition of periodic boundary conditions in Eqs. (3.1) necessitates the creation of *pairs* of kinks and antikinks. On these steps, the number of K K collisions cannot be sustained as the current is lowered further. The final K K is stable above $\Gamma_0 \approx 0.08$, while below this critical driving strength, dissipation dominates, and no current flows. In the low voltage regime, there the

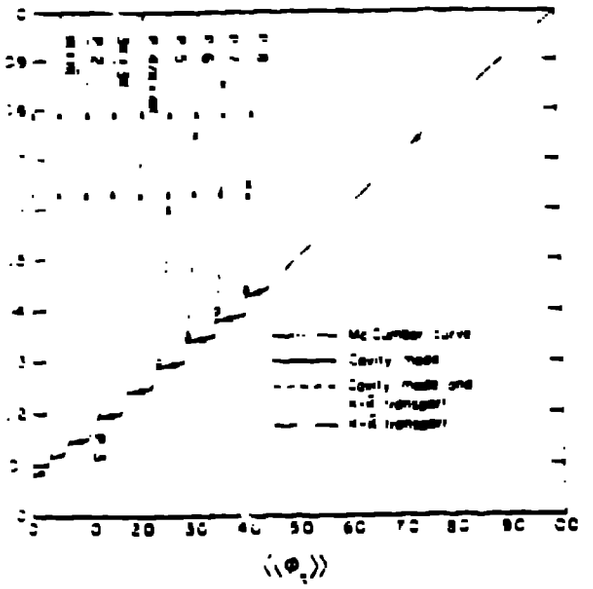

Figure 7. A summary of numerical results. The arrows indicate the direction in which the driving, Γ_0, was adiabatically changed. The c's on the periodic steps (labeled P-N) denote where the periodic symmetry breaks to another P-N state (see Fig. 8) when Γ_0 is increased, and the o's indicate where the symmetry is regained as Γ_0 is decreased. Notice that for $0.15 \leq \Gamma_0 \leq 0.18$ on the 3K-3K step, the spatial pattern is periodic.

exist one additional phase-locked state with spatial period equal to two. This mode is also unusual in that the other states appearing in Fig. 7 may be accessed by evolving a random-spatial profile according to Eqs. (3.1) with an appropriate Γ_0. For the period-two state manner. These observations lead us to believe that the length of our system is nearly consistent with an exact period-two solution to the SG equation, subject to periodic boundary conditions.

This system also possesses a regime where the two types of transport yield the same I-V characteristic, viz., the period-four (P-4) and 4K-4K curves of Fig. 7 (... and 9(b)). On this step, the P-4 structure was obtained by adiabatically increasing Γ_0, while the 4K-4K state was generated by setting $\Gamma_0 = 0.30$ and ... initial state with a random spatial profile. We found that these coexisting ... Eqs. (3.1) are mutually stable with respect to spatially homogeneous ... (including point impurity-type perturbations with strengths up to 0.2Γ ... that both type ... transport mechanisms display the same I-... necessary to measure some other quantity, such as the power ... distinguish between them.

... generating Fig. 7, it is evident that Eqs. (3.1) ... spatial pattern ... simply changes with a small change in ... opposite direction, does not recover the previous state. Instead, ... the state with the new spatial pattern, and a new current ... In addition to this large-scale hysteresis, there is ... activity that occurs ... the higher steps. On the high voltage ... the simple stripe ... in Fig. 8 is replaced by an ... incommensurate looking ... contains interleaved breathing ... Figs. ... This symmetry breaking ... the spatial pattern, ... However, if the ...

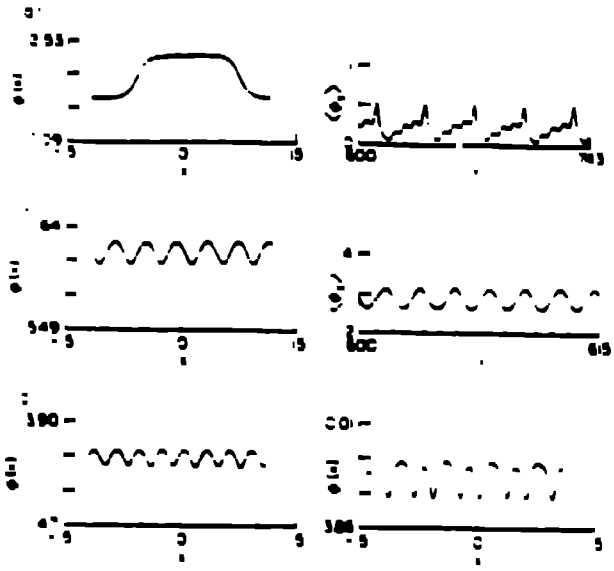

Figure 5. In each of the cases presented, the value of ϕ is given *modulo* 2π. In each case, the difference between the top and the bottom of the graphs is 15 units. a) The 1K – 1K state. Here, transport is due to the transverse motion of the kinks, and results in the lowest step in Fig. 7. b) The P-6 state. Here, transport is due to the running average of the phase-locked wave train, as can be seen in the space-vs-time plot on the right. (Period 1) On the left-hand side are the P-6 and P-5 spatial states that are stable for low driving. On the right-hand side are the symmetry-broken states obtained when the driving is increased beyond 0.75 and 0.65, respectively.

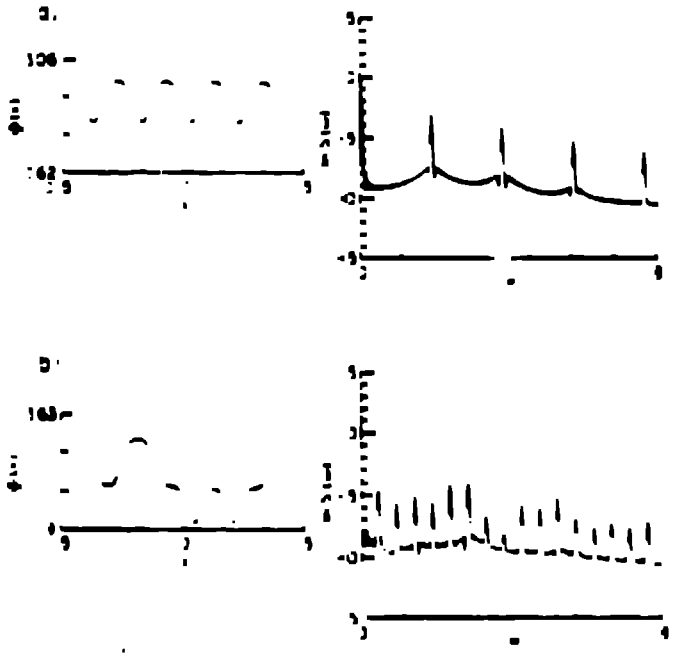

driving is reduced to near, but before, the onset of the step (see Fig. 7, where the x's represent approximately where the symmetry breaks with increasing Γ_0, and the o's represent where the symmetry is regained with decreasing Γ_0). We believe that this breaking of the spatial pattern is caused by the multibreather-wave-train nature of the cavity-mode states, which results in a *competition* of length scales. Since the amplitude and width of a breather are related to its internal frequency, and the applied current drives this frequency, the system eventually reaches a point where it is energetically favorable for it to create a second type of breather to relieve the internal stress.

It is helpful to contrast these ZFS structures with those that occur in overlap-geometry Josephson junctions. As we mentioned earlier, the imposition of periodic boundary conditions guarantees that only K-K pairs will be excited, so that only even steps are generated from the uniform spatial state. The patterns that we observe, cavity modes and fluxon-antifluxon pairs, are simpler than the symmetric and asymmetric modes that are obtained with Neumann boundary conditions.

Analytic treatments of this system are possible in principle both in terms of linear stability analysis and in a soliton basis -- indeed the system is sufficiently simple that it should be a valuable testing ground for nonlinear collective mode reductions in the presence of perturbations.

Linear stability of the spatially homogeneous rotating state to a period-N, cavity mode state is furthest developed to date -- at least for onset conditions; the nonlinear saturation of period-N linear modes requires fully a nonlinear mode basis. Linear stability analysis starts with the spatially uniform solution to the unperturbed SG equation and adds a perturbation of the form $y(t)f(x)$, where $f(x)$ is periodic. When this solution is substituted into Eq. (3.1) and the result is linearized, we get

$$f''(x)y(t) - f(x)\ddot{y}(t) - f(x)y(t)\left[1 - 2sn^2\left[\frac{t}{\alpha};\alpha\right]\right] = -f(x)\ddot{y}(t) + \left[\dot{\phi}_0(t) - \Gamma_0\right], \tag{3.2}$$

where $sn(u,\alpha)$ is a Jacobi elliptic function, α is the modulus of this function, and

$$\dot{\phi}_0(t) = \frac{2}{\alpha}\left[1 - \alpha^2 sn^2\left[\frac{t}{\alpha};\alpha\right]\right]^{1/2}.$$

Next, write $f(x)$ as

$$f(x) = \sum_n f_n e^{imkx}, \tag{3.3}$$

where $k = 2\pi/L$ and N is the spatial periodicity of the final state. When we multiply Eq. (3.2) by $\exp(imkx)$ and integrate over x, we get (with $f_m \neq 0$)

$$\ddot{y} + \left[\alpha^2 m^2 k^2 + 1 - 2\alpha^2 sn^2\left[\frac{t}{\alpha};\alpha\right]\right] y(t) = \Gamma_0 - \dot{\phi}_0(t).$$

The resulting equation can be solved perturbatively by expanding $\alpha^2 = \frac{1}{2} + \varepsilon$ as explained in [20]. This approach is correct for $\alpha^2 \ll 1$ (quantitatively improves

the transition points between uniform and period-N or period-N and period-(N−1) states.

Attempts to use a full soliton mode basis are in progress [27]. These exploit the integrability of the unperturbed SG equation, as discussed in section 2. The nonlinear spectral transform can be used to characterize the various branches in terms of their KK, breather and radiation components. Various analytic perturbation schemes can then be used to describe the time evolution of, e.g., Θ-function representations [27] under our perturbations. Correspondingly, we have also used the nonlinear spectral scheme described in section 2 to numerically follow the various soliton components −− this involves some subtlety of interpretation to separate a rotating background from additional dynamic spatial structure.

Finally, we mention that this (1+1)-dimensional SG system can be used to approximately model *wall* dynamics in (2+1)-dimensional, discrete SG problems. This is accomplished by describing the fluctuations relative to the wall center of mass, as described in ref. [28]. Correspondingly wall motion in (N+1)-dimensional SG can be reduced approximately to a (N−1)+1)-dimensional system. In this way the phenomena described in this section model the propagation of walls by *transverse* pattern formation −− e.g. transverse KK nucleation, as observed in dislocation motion in crystals. Analysis of transverse patterns on propagating interfaces is important in many fields (e.g. cellular textures on flame fronts) and is likely to receive further attention experimentally in condensed matter settings −− for instance domain wall motion in hard magnetic materials.

4. The (1+1)-Dimensional SG Model with Nonconvex Interparticle Interactions

As we mentioned in the Introduction, solid state physics in the last 15 years has rediscovered the SG equation in the context of commensurate-incommensurate phase transitions now observed experimentally in very many kinds of materials [3]. In these situations, several length scales are in competition and lead to intrinsically inhomogeneous ground states (frequently, ordered or irregular arrays of kink-solitons).

Most of the theoretical studies to date have concentrated on cases where the interparticle interactions are *convex*, as in the *discrete* version of the SG equation (2.1c). A typical case is where there are *two* competing lengths: the lattice constant between an array of particles (e.g. atoms) and a periodic potential in which they sit with a periodicity which is incommensurate with the lattice constant.

Recently, motivated by physical concerns, the class of problems has been extended to include *nonconvex* interactions between particles leading to additional, and qualitatively different, competing length scales [29]. Nonconvex interparticle interactions can arise effectively in a Ginzburg Landau free energy functional for the strain (differences in displacements between neighboring particles) in materials which undergo elastic phase transitions. The model described below may, for example, be useful in descriptions of twin boundary dynamics in martensitic materials [29]. Here the substrate potential models, e.g., the parent phase and other terms describe an expansion of the elastic free energy as a function of the strain and strain gradients.

One model which has been studied in some detail [29] is

$$H = \sum_n \frac{1}{2} \left(\frac{du_n}{dt} \right)^2 + \frac{1}{2} \left(u_{n+1} - u_n \right)^2 + \frac{1}{4} \left(u_{n+1} - u_n \right)^4$$

$$+\frac{1}{2}\gamma(u_{n+1}-2u_n+u_{n-1})^2-\cos u_n\ . \qquad (4.1)$$

Here, there is a competition between the substrate periodicity 2π and the natural lattice constant $2\pi\ell_0$, $\ell_0^2 = A/2\alpha$. Further generalizations are given in [29]. It is easy to see that for $\gamma \ll 1$ the system will behave as for $\gamma = 0$ with $A \to A-2\gamma$. The ground state is then *dimerized* (i.e. a periodic line of "short" and "long" lattice constants) for $A-2\gamma > \frac{1}{8}$. On the other hand, for large values of α, A, γ (i.e. when the substrate is weak), it can be shown [29] that a long-period superlattice (a "kink-antikink" or "twinning" [30] pattern) is formed and stabilized by the substrate competition. Roughly these patterns are a periodic array of N short lattice constants, followed by M long ones, with the (N+M) unit cell periodically repeated. N and M are integers and may be equal.

The detailed ground state phase diagram has been obtained [29] by a combination of ansatz, numerically exact transfer integral techniques, and numerical relaxation of the equations of motion following from (4.1) The results (for $\ell_0 \ll 2\pi$, so that the dominant nonlinearity is in the interaction potential and SG "solitons" are not important) are summarized in fig. 10. The notation in this figure is given in the figure caption. We draw attention to two interesting features: (1) The transition from the uniform to long-period ground states contains at worst a triple point (three coexisting phase) and possibly a Lifshitz point character; (2) Transitions between long-period ground states are typically first-order, not continuous. These results distinguish model (4.1) from, e.g., the Frenkel-Kontorova model and are a direct consequence of the interparticle *nonconvexity*. In particular the interactions between defects ("solitons") within each long-period pattern (see fig. 10) is attractive leading to the nucleative first order character. This is in contrast with the convex interaction case, where the interaction is repulsive, giving rise to a soliton lattice (incommensurate structure) with a *continuous* transition in the soliton spacing. The soliton nucleation transition mechanism pre-empts an alternative "soft mode" (or "phonon-mediated") scenario in which the period of the patterns could change homogeneously and continuously: this can happen in principle because of the competing first- and second-neighbor gradient terms. The exceptions to this rule are transitions from that *uniform* ground state. Linearizing we find that $\omega(q) \sim -q^2 + q^4$, when $-q^2$ is not stabilized by q^4, a transition can occur. Specifically [29], linear stability shows two regimes: (a) $\gamma < 1/16$, where the homogeneous state becomes unstable and bifurcates into a dimerized one along the line $A = 2\gamma + \frac{1}{8}$; and (b) $\gamma > 1/16$, where the homogeneous state becomes unstable along the curve $A = \alpha^{1/2}$ and bifurcates into modulated states with wavenumber $q_c = (2\pi)^{-1}\cos^{-1}(\frac{1}{2}\gamma^{-1/2}) < 1$.

an infinite number (incomplete "Devil's staircase") of both commensurate and incommensurate ground phases. As stated above, a corresponding linear stability analysis of the modulated phases themselves shows that the actual (nucleation driven) phase boundaries may lie *inside* the domains of linear stability. The strong hysteresis accompanying these transitions can be clearly seen in numerical relaxations studies as parameters are adiabatically varied.

The complex ground state structure and first order transitions naturally lead to highly hysteretic, multiple time scale dynamics. Indeed, this model will be a excellent template for analyzing solitary wave transport and response in computer interaction problems as discussed in section 3. Dynamic studies to date [29] include analysis of the optic and acoustic phonons accompanying the homogeneous ground state, relaxation of localized thermodynamic mutual conditions shown in

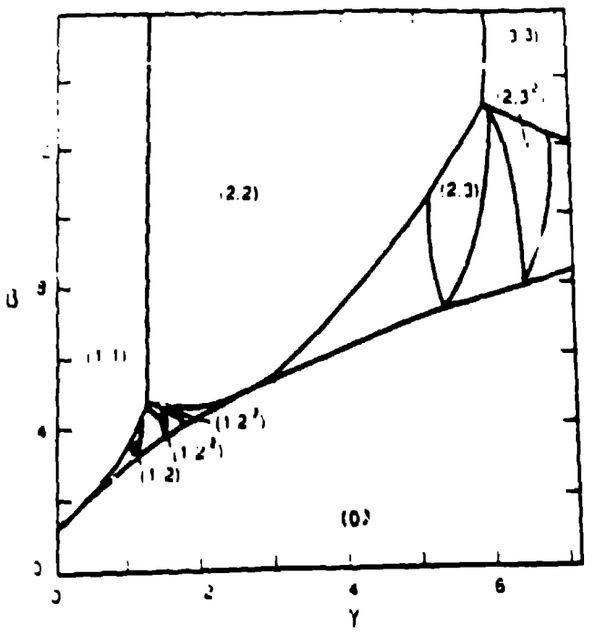
(2.2)
(2.3)
(1 1)
(1 2²)
(1 2²)
(1 2)
(0)
Y

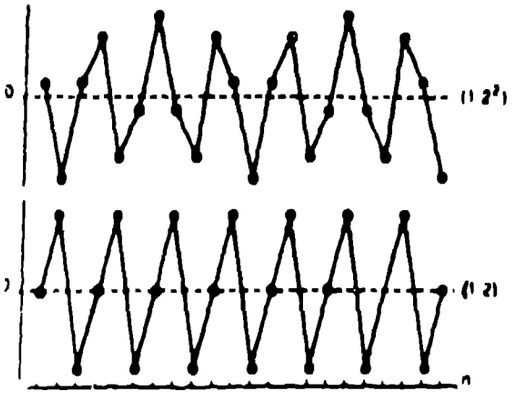
(1 2²)
(1 2)

importance of pinning effects which lock defects randomly in the true ground state; and (3) effects of a DC-field and damping. Point (3) is extremely interesting and appears to contain the ingredients of "1/f" noise and a relationship between time *and* space characterizations of this phenomenon. Indeed this "noise" occurs through the motion of local defects, a notion which is now rising even in theories of fully developed turbulence [31]. Comparison with the DC-driven SG system of section 3 is instructive. There, linear stability analysis of the *uniform* rotating state identified periodic wave-train unstable modes, which saturated into breather and KK wave-trains. Here, the rotating state is itself inhomogeneous because of the internal ground state complexity [29]. Linear stability analysis then shows that this state destabilizes through *local* modes being excited and saturating in the nonlinearity as the rotation rate decreases and allows the complex landscape of metastable pinned configurations to be felt. These modes contain explicit frequency- and spatial-scale relationships. In this sense the rigidly rotating state is "critically unstable" [32] as the rotation rate is decreased to a critical value and is destabilized by a low density of defects (with respect to the rotating pattern) being excited and moving slowly relative to the average rotation rate —— they then control long-wavelength and long-time character in a *connected* way, giving rise to 1/f behavior. We can expect that the "critical" properties will be very interesting, as discussed in other competing interaction systems with critical transport in the presence of DC-driving [11].

5. Quantum Dynamics of a Pulsed Spin System

In this section we introduce some recent approaches to *quantum* mechanics of systems with interesting (e.g. chaotic) classical limits. This field (often equally referred to as "quantum chaos") is associated with its own considerable history and literature. Our intention in the model problem introduced below is quite limited. We wish to emphasize in the context of this Institute that: (a) Competing interactions are equally important in quantum problems as in classical ones; (b) It is very important to have control of models which contain an integrable limit and where deviations from integrability can be "tuned," as for classical models; and (c) It is natural to try to characterize such quantum problems by scaling and "fractal" measures, analagous to the successful approaches developed for classical limits. Furthermore, this includes studying wave function and dynamics as well as more traditional investigations of energy level distributions.

Considering quantum *dynamics*, we can expect that the coherent structure of wavefunctions is greatly affected by quantum interference, leading to the suppression of anomalous diffusion features characteristic of chaos and eventually to the vanishing of the Kolmogorov Sinai entropy and of other characteristic exponents. If we consider the semi-classical regime, however, new phenomena can appear, not present in either the classical or quantum limit. In particular, semiclassical wavefunction patterns may exhibit several distinctive behaviors in a recurrent time regime beyond the so-called Ehrenfest time t_E at which the classical and quantum correspondence breaks down. In the case of hyperbolic fixed points of the corresponding classical motion, the classical Lyapunov exponents $\lambda_1, \lambda_2 = \pm\lambda$ (See, e.g. [33]). But these behaviors have so far been examined systematically, most previous studies on the dynamics of wavefunctions have concentrated on the time regime $t < t_E$. For a study of long time and semiclassical behaviors, quantum large spin systems are especially advantageous because the finite dimensionality of their Hilbert space requires the explicit quantization of the key matrices. In order for our proposed experiment to be

spin resonance, for instance, an assembly of spin 1/2 systems behaves coherently and effectively constitutes a single large quantum-spin.

Here, we report on the long-time behavior of wavefunctions in a periodically-pulsed large quantum-spin system whose classical limit exhibits a transition from predominantly regular orbits to global chaos as the pulse strength is increased. The effect of dissipation is omitted in the present treatment. We shall attempt to characterize wavefunction patterns in terms of their singularity spectra $f(\alpha)$, which has proven very useful recently in quantifying many essential aspects of chaotic systems [34].

The quantum dynamics for our spin system with $\vec{S} = (S^x, S^y, S^z)$ is described by $i\hbar\dot{\Psi} = H\,\Psi$ where $H = H_0 + \sum_{n=-\infty}^{\infty} V\,\delta(t - 2\pi n)$ with $H_0 = A(S^z)^2$ and $V = \mu B S^x$. A (>0) and μB (>0) represent a planar anisotropy and pulse strength, respectively. (Here we have chosen a convenient model Hamiltonian. One may make other choices, e.g., $H_0 = AS^z$ and $V = -\mu B S^x \cos(\omega t)$, without changing the qualitative features of the results below.) We solve the above Schrödinger equation by rewriting it immediately in a matrix form: a set of eigenstates of S^z is chosen as basis kets. Then, the wavefunction Ψ just after the n-th pulse is given by $\Psi(2\pi n + 0) = \sum_{m=-S}^{S} C_m(2\pi n + 0)\,|\,m\,\rangle$ with $C^i(2\pi n + 0) = \sum_a \exp(-2\pi i n E_a/\hbar)\cdot(\vec{X}_a \cdot \vec{C}(+0))\vec{X}_a$. Here $\{E_a\}$, $\{\vec{X}_a\}$ are quasi-energies and quasi-eigenfunctions for the one period propagator represented by the unitary matrix: $U = \exp(-(i/\hbar)V)\exp(-(i/\hbar)2\pi H_0)$. V and H_0 are matrices for V and H_0, respectively. The probability density function is given in terms of SU(2S + 1) coherent state representations as $P_n(\theta,\varphi) = [(2S+1)/4\pi]\,|\langle\theta,\varphi|\,2\pi n + 0\,\rangle|^2$, where the first factor on the right-hand side is due to the normalization over the surface of a unit radius sphere. In the following, $A = 1.0$ sets the energy unit. Further, we employ $S = 128$ and choose $\hbar = 1/\sqrt{S(S+1)}$ so that the observable spin magnitude maintains the scaled value for the classical spin vector, i.e., $S^2/S(S+1)\hbar^2 = 1$.

In fig. 1, very early stages ($n = 1, 2, 3$) of the temporal evolution of initially ($n = 0$) localized wavepackets are shown. For a weak pulse ($\mu B = \mu B/A = 0.01$), $P_n(\theta,\varphi)$ shows a simple unidirectional diffusion (see figs. 1(a) - (c)) corresponding to regular behaviors in classical dynamics. (Note that investigation of classical dynamics indicates the presence of two characteristic fields $\mu B_1 \sim 0.1$ and $\mu B_2 \sim 0.5$ above the fraction of chaotic trajectories increases strongly and the last KAM torus disappears, respectively.) However, for a strong pulse ($\mu B = 1.0$), remarkable stretch and irregular diffusion begin after the period of "classical" stretch-and-folding type diffusion. Fig. 1 also indicates $t_c \sim 0(1)$ for both the $\mu B = 0.01$ and 1.0 cases. The above results resemble a quantized version of chaotic dynamical systems (e.g., Chirikov's standard map) in which wavefunctions have been reported [35] to exhibit highly singular patterns after stretching and folding. Very certain eigenstates were found with anomalous localization lengths.

We now proceed to examine $P_n(\theta,\varphi)$ in later regions ($n = 50, 90, 130, \ldots$) of the $\mu B = 1.0$ case. While the exact classical-quantum correspondence has been lost in this time region, the evolutions clearly manifest some traces of the underlying chaotic dynamics (figs. 2(a) - 2(c), 3(a) - 3(c), and 4(a) - 4(c)). Such regions, in which

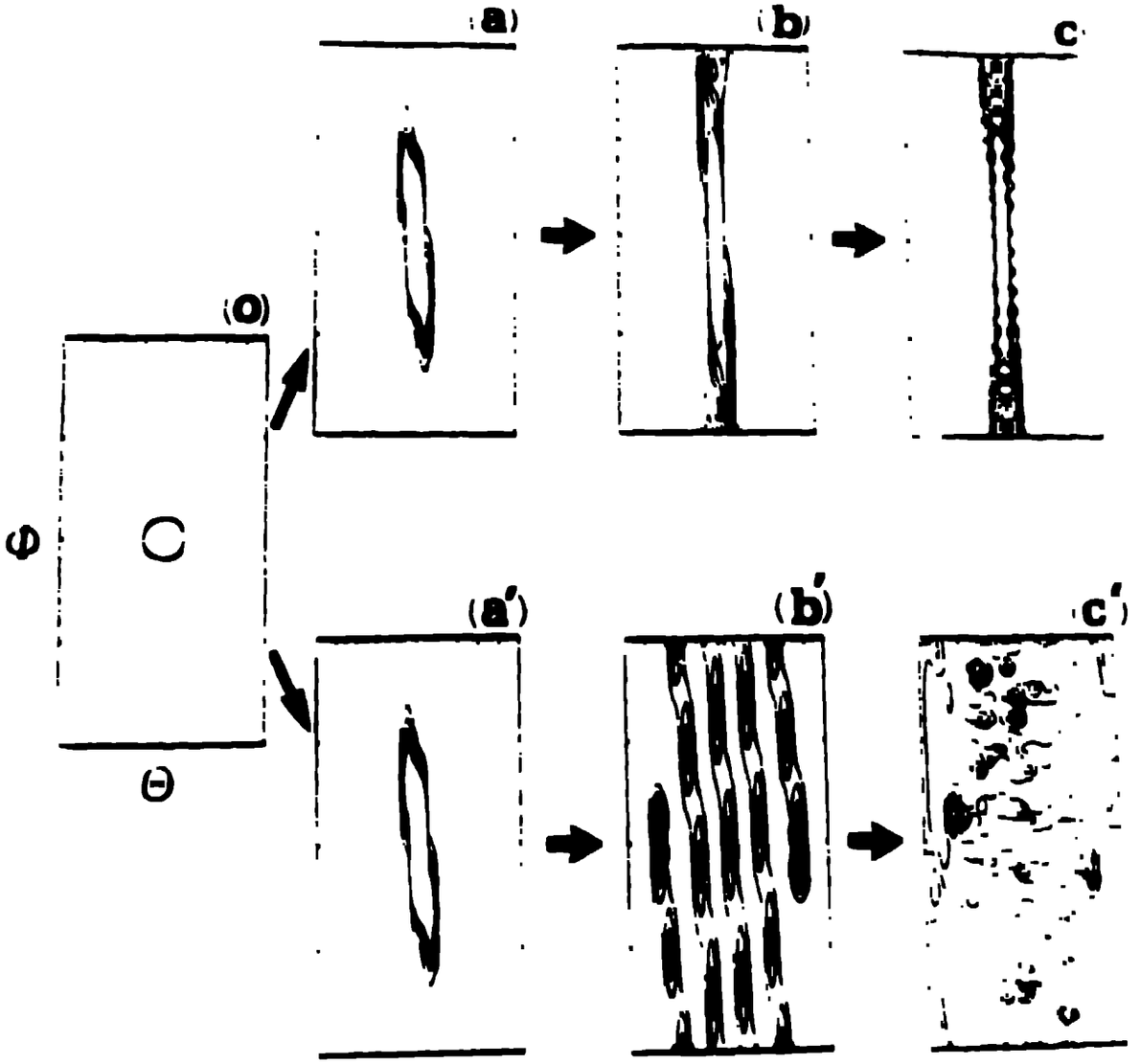
(a)
(b)
c
(o)
Φ
C
Θ
(a′)
(b′)
c′

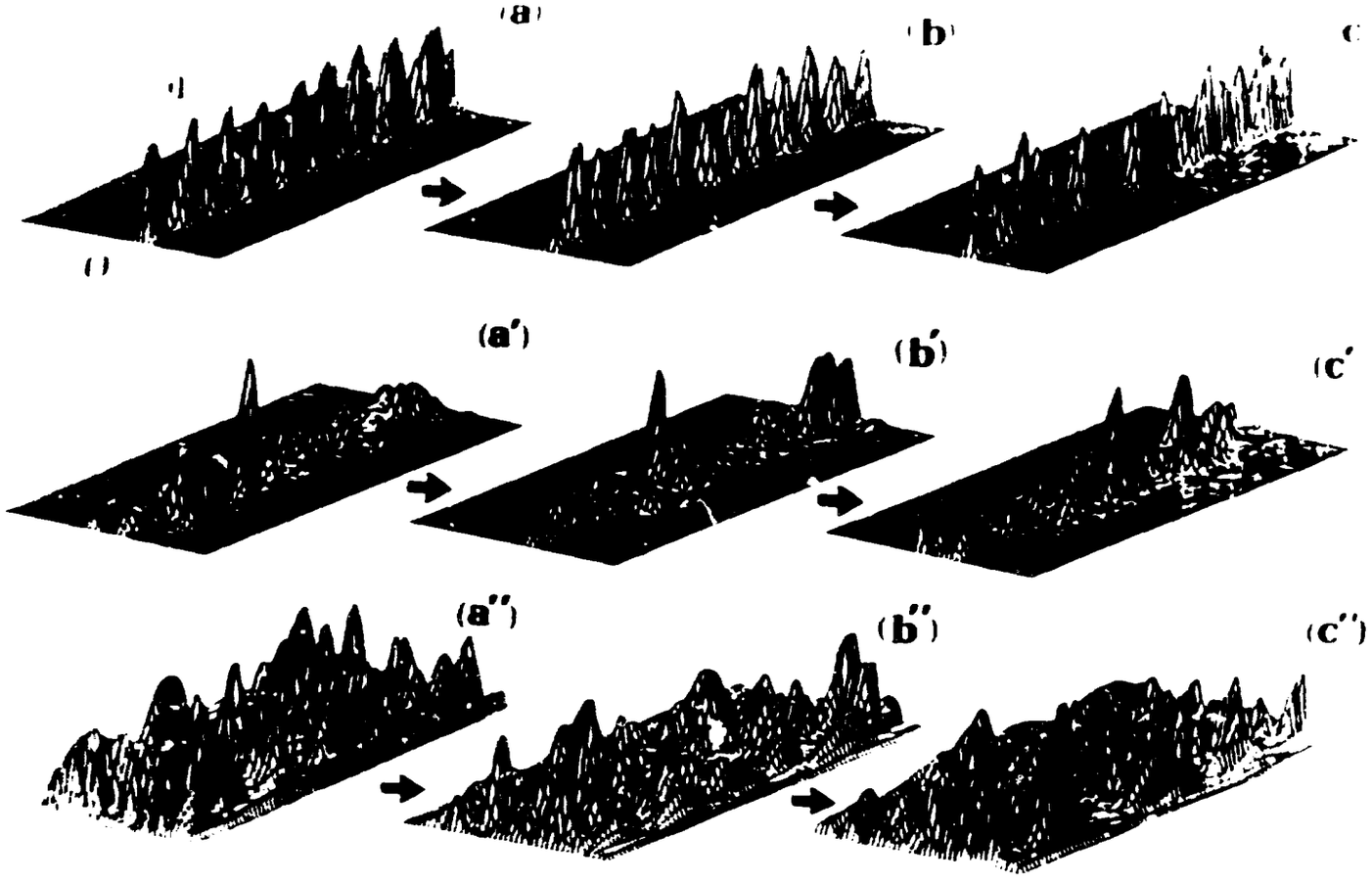

Evolution of 3D profiles of $P_{\alpha\beta}(\theta_{\alpha\beta})$ for [illegible] with B
[illegible] From the left to 70, 90 and 110

to [illegible] x2 [illegible] 1.2, [illegible] = 0 S [illegible]. The scaling exponents τ_q [illegible] obtained [illegible]. It should be noted, however, that our numerical data P_n [illegible] only to the order of 10^{-7}. Using them as inputs, we can obtain [illegible] for [illegible] in the case $q \geq 0$, but [illegible] is difficult to explore sufficiently [illegible] regions in the case $q < 0$. So our reports of $f(\alpha)$ below will be limited to $q \geq 0$. This restriction does not prevent us from studying the general tendencies of fluctuations of singularities or local dimensions α. Fig. 13 represents $f(\alpha)$ with $q \geq 0$ for several μB values at [illegible] fixed time $n = 30$. We find that fluctuations of α for μB = [illegible] and 1.0 fall into a narrow range and those for $\mu B = 0.2$ extend over a much wider range. The large fluctuation in the latter case signifies the inhomogeneous distribution of measure $P_n(\theta)$ [illegible] Fig. 12 (b), which

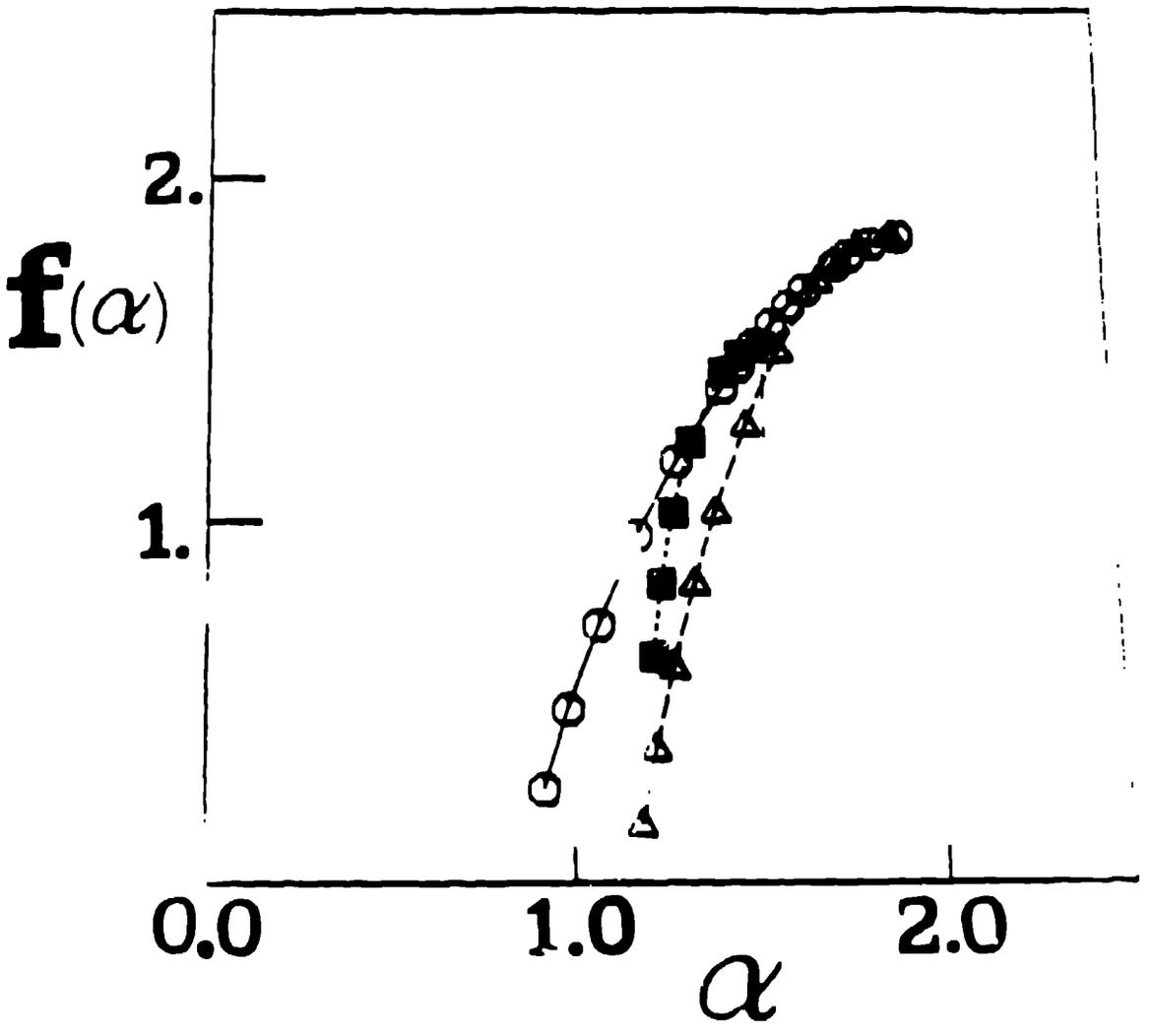

[illegible]

reflects the coexistence of classical KAM orbits and localized chaos in a transitional region leading to global chaos. This large fluctuation is reminiscent of the critical fluctuations at an equilibrium phase transition. The relatively small fluctuation for $\mu\tilde{B} = 1.0$ signifies the uniform distribution of measures in Figs. 12(b'').

Using our data for $f(\alpha)$ with $q \geq 0$, we now estimate the effective range of fluctuations $\alpha^*_{min} \leq \alpha \leq \alpha^*_{max}$: α^*_{max} and α^*_{min} denote the value at which $f(\alpha)$ takes the maximum (i.e., fractal dimension) and the value at which $f(\alpha)$ takes 2/3 times its maximum (an arbitrary choice). For $\mu\tilde{B} = 0.2$ at n = 90, for example, $\alpha^*_{max} = 1.98 \pm 0.01$, $\alpha^*_{min} = 1.35 \pm 0.01$. The features in fig. 13, which have now been quantified, are found to persist throughout the temporal evolution. Careful examinations indicate: (1) the effective range of α shows distinctive temporal variations for $\mu\tilde{B} = 0.2$; (2) on the other hand, it remains almost unchanged for $\mu\tilde{B} = 1.0$ (despite the absence of dissipation in the present system), which reflects a well-organized ergodicity in this case.

The mixing and ergodic features of classical chaos have helped to establish relationships with the formalism of equilibrium statistical mechanics. In the field of quantum chaos, most of the literal definitions of classical chaos lose their significance. Nonetheless, we have still found here complicated behaviors in the quantum mechanical treatment of chaotic systems. We believe that the characterization given here will be a vehicle for more profound understanding of these complexities. Summarizing, despite the complete absence of classical and quantum correspondence, the long-time behavior of semiclassical wavefunctions maintains the ergodic and nonergodic features possessed by the underlying classical dynamics. The enhanced fluctuation of their local dimensions in a transitional region leading to global chaos persists throughout the time evolution. This is reminiscent of critical fluctuations at an equilibrium phase transition.

6. Summary

In summary, studies of complexity in models motivated by condensed matter and materials science have focused attention on a number of issues of wide importance in dynamical systems: (i) The importance of understanding complexity in extended (space-time) systems, so that *interrelations* of pattern formation and complicated dynamics can be included; (ii) The fundamental role played by *competing interactions*, including both length scales and frequencies; (iii) ***Mappings*** between time-dependent, nonequilibrium systems (pde's, neural networks, coupled map lattice, cellular automata), and to effective, equilibrium Hamiltonian systems in higher spatial dimensions and with competing length scales. (Excellent examples are found in the liquid crystal convection cell experiments of Ribotta (see these proceedings)); (iv) The value of *nonlinear* collective (e.g. soliton-like) *mode reduction* as a basis for describing low dimensional attractors in many degree-of-freedom systems; (v) The role of generalized (space-time) *homoclinic orbits* for describing the geometry of both temporal sensitivities and spatial instabilities; and (vi) The important role played by "defects" in controlling the large scale flow (transport) of competing interaction systems.

From a theoretical perspective, a number of techniques have been developed and tested on specific models with which to describe aspects seen in real or numerical experiments: e.g. perturbation theory around linear and nonlinear states [37]; perturbation theory in a collective coordinate or soliton basis [38]; energy balance criteria for nonlinear modes [39]; algorithms for computing ground state

in the presence of competing interactions [29], etc. Much development remains necessary, however, in terms of, e.g., incorporating collective coordinates in Renormalization Group or Fokker-Planck descriptions, controlling estimates of center manifold dimensionality, describing energy transfer between nonlinear modes, analyzing frequency and phase "pulling" of coupled nonlinear oscillator, understanding coexisting homoclinic orbits and their connections, including effects of noise and disorder in nonlinear systems [40], describing dynamics in competing interaction systems, etc.

Finally, while the precision, elegance and variety of condensed matter experiments which probe "complexity" in time and space have increased dramatically, it should be remembered that a plethora of phenomena in mainstream *metallurgy* share similar features [2]. We expect that a great deal of attention will soon focus on microscopic modeling of texturing and of nontrivial dynamics in material science, and on the bridge to condensed matter, where we have gained some understanding via simpler, controlled systems.

We gratefully acknowledge close collaborations over the last several years with many colleagues, including S. Aubry, J. Ariyasu, G. Forest, P. Lomdahl, S. Marianer, A. Mazor, D. McLaughlin, K. Nakamura and E. Overman, II.

REFERENCES

1. "Spatio-temporal coherence and chaos in physical systems," eds. A. Bishop, G. Gruner, B. Nicolaenko (North-Holland, 1986).

2. "Competing interactions and microstructures: statics and dynamics," eds. R. LeSar, A. Bishop, R. Heffner (Springer-Verlag, 1988).

3. P. Bak, Rep. Phys. **45**, 587 (1982).

4. See, e.g., articles in Ref. 2.

5. E. A. Overman, II, D. W. McLaughlin and A. R. Bishop, Physica D **19**, 1 (1986).

6. A. R. Bishop, D. W. McLaughlin, M. G. Forest and E. A. Overman, Jr., Phys. Lett. **127A**, 335 (1988).

7. K. Nakamura, A. R. Bishop et al. Phys. Rev. Lett. **54**, 861 (1985); Phys. Rev. Lett. **57**, 5 (1986); Phys. Lett. **117A**, 459 (1986); Phys. Rev. B, in press (1989).

8. A. C. Scott et al, preprint (1989).

9. R. Eykholt, A. Bishop, P. Lomdahl and E. Domany, Physica **23D**, 102 (1986).

10. A. R. Bishop, J. A. Krumhansl and S. E. Trullinger, Physica **1D**, 1 (1980).

11. A. R. Bishop, B. Horovitz and P. S. Lomdahl, Phys. Rev. B **38**, 4853 (1988).

12. A. R. Bishop and P. S. Lomdahl, Physica **18D**, 54 (1986).

13. A. R. Bishop et al, Phys. Rev. Lett. **50**, 1095 (1983).

14. See, M. G. Forest and D. W. McLaughlin, J. Math. Phys. **73**, 1248 (1982).

15. N. M. Ercolani, M. G. Forest, and D. W. McLaughlin, Physica D (in press).

16. C. R. Doering, J. D. Gibbon, D. D. Holm and B. Nicolaenko, Nonlinearity **1**. 179 (1988).

17. D. W. McLaughlin, private communication.

18. N. M. Ercolani, M. G. Forest and D. W. McLaughlin, preprint (1988).

19. J. C. Ariyasu and A. R. Bishop, Phys. Rev. B **35**, 3207 (1987).

20. e.g. J. Guckenheimer and P. Holmes, "Nonlinear Oscillations, Dynamical Systems, and Bifurcations of Vector Fields," (Springer-Verlag 1983).

21. A. R. Bishop et al, Phys. Lett A (in press) (1989), and preprint (1989).

22. G. Kavacic and S. Wiggins, preprint (1988).

23. D. David, D. D. Holm and M. V. Tratnik, Phys. Lett. **137A**, 355 (1989); and Physics Reports (in press).

24. J. C. Ariyasu and A. R. Bishop, Phys. Rev. A (in press) (1989).

25. M. Salerno, Phys. Lett A (in press) (1989).

26. See ref. 24.

27. R. Flesch, M. G. Forest and A. Sinha, in preparation.

28. J. Pouget, S. Aubry, A. Bishop and P. Lomdahl, Phys. Rev. B (in press) (1989).

29. S. Aubry, K. Fesser and A. R. Bishop, J. Phys. A **18**, 3157 (1985); S. Marianer and A. R. Bishop, Phys. Rev. B , (1988); M. Floria and S. Marianer, Phys. Rev. B (in press); A. R. Bishop, S. Marianer and M. Floria, preprint.

30. G. Barsch, B. Horovitz and J. Krumhansl, Phys. Rev. Lett. **59**, 1251 (1987).

31. e.g., H. Chaté, these proceedings.

32. e.g. P. Bak and C. Tang, Physics Today **42**, S27 (1989).

33. M. V. Berry and N. L. Balazs, J. Phys. **A12**, 625 (1979).

34. e.g. T. Halsey et al, Phys. Rev. **A33**, 1141 (1986).

35. N. L. Balazs and A. Voros, Europhys. Lett. **4**, 1089 (1987), and Annals of Phys. (in press).

36. R. Ribotta and A. Joets, these proceedings.

37. e.g. A. Mazor and A. R. Bishop, Physica **27D**, 269 (1987); D. W. McLaughlin, A. Pearlstein and G. Terrones, preprint (1988).

38. N. M. Ercolani, M. G. Forest and D. W. McLaughlin, Lectures in Appl. Math. **23**, 3 (1985) and preprint (1988).

39. P. S. Lomdahl and M. R. Samuelson, Phys. Rev. B, (1985).

40. "Disorder and Nonlinearity," eds. A. R. Bishop, D. K. Campbell and S. Pnevmatikos (Springer-Verlag 1989).